Article:
van Zuilen, K, Mueller, T orcid.org/0000-0002-1045-2110, Naegler, T et al. (2 more authors) (2016) Experimental determination of barium isotope fractionation during diffusion and adsorption processes at low temperatures. Geochimica et Cosmochimica Acta, 186. pp. 226-241. ISSN 0016-7037

https://doi.org/10.1016/j.gca.2016.04.049

Experimental determination of barium isotope fractionation during diffusion and adsorption processes at low temperatures

Kirsten van Zuilen [a,*], Thomas Müller [b], Thomas F. Nägler [a], Martin Dietzel [c] and Tim Kuesters [b]

[a] Institute of Geological Sciences, University of Bern, Baltzerstrasse 1+3, 3012 Bern, Switzerland

[b] Institute of Geophysics and Tectonics, School of Earth and Environment, University of Leeds, Leeds, LS2 9JT, UK

[c] Institute of Applied Geosciences, Graz University of Technology, Rechbauerstraße 12, 8010 Graz, Austria

*Corresponding author: kirsten.vanzuilen@geo.unibe.ch

Present address: Institut de Physique du Globe de Paris, 1 rue Jussieu, 75238 Paris cedex 05

Manuscript submitted to GCA on 22 September 2015

Keywords: Barium, Ba isotopes, diffusion, adsorption, stable isotope fractionation, experiment, diffusive transport model, reactive transport

Abstract

Variations in barium (Ba) stable isotope abundances measured in low and high temperature environments have recently received increasing attention. The actual processes controlling Ba isotope fractionation, however, remain mostly elusive. In this study, we present the first experimental approach to quantity the contribution of diffusion and adsorption on mass-dependent Ba isotope fractionation during transport of aqueous Ba^{2+} ions through a porous medium. Experiments have been carried out in which a $BaCl_2$ solution of known isotopic composition diffused through u-shaped glass tubes filled with silica hydrogel at 10 °C and 25 °C for up to 201 days. The diffused Ba was highly fractionated by up to -2.15 ‰ in $\delta^{137/134}$Ba, despite its high atomic mass. The time-dependent isotope fractionation can be successfully reproduced by a diffusive transport model accounting for mass-dependent differences in the effective diffusivities of the Ba isotope species ($D_{^{137}Ba}/D_{^{134}Ba} = (m_{134}/m_{137})^{\beta}$). Values of β extracted from the transport model were in the range of 0.010 to 0.011. Independently conducted batch experiments revealed that adsorption of Ba onto the surface of silica hydrogel favoured the heavier Ba isotopes (α = 1.00015 ± 0.00008). The contribution of adsorption on the overall isotope fractionation in the diffusion experiments, however, was found to be small. Our results contribute to the understanding of Ba isotope fractionation processes, which is crucial for interpreting natural isotope variations and the assessment of Ba isotope ratios as geochemical proxies.

1. INTRODUCTION

Barium (Ba) has received attention in the past as geochemical proxy in both low and high temperature environments. In the oceans, precipitation of barite ($BaSO_4$), being the main carrier of particulate Ba in the water column, is associated with the decay of planktonic organic matter (Bishop, 1988; Dehairs et al., 1980; Ganeshram et al., 2003; Goldberg and Arrhenius, 1958). Consequently, export fluxes of C_{org} and Ba from the water column are positively correlated (Dymond and Collier, 1996; Dymond et al., 1992). Based on this correlation, Ba accumulation rates in marine sediments have been widely used to reconstruct paleo-productivities (e.g., Dymond et al., 1992; François et al., 1995; Hull and Norris, 2011; Paytan et al., 2007; Paytan and Griffith, 2007; Paytan and Kastner, 1996). The validity of this proxy, however, must be questioned for samples derived from sediments, where microbial sulphate reduction has taken place, as barite remains no longer stable (McManus et al., 1998; Paytan and Griffith, 2007).

Due to the flux of particulate Ba to the seafloor and hydrothermal activity (e.g., Cronan and Hodkinson, 1997; Dymond et al., 1992), Ba is strongly enriched in marine sediments relative to mid-ocean ridge basalt (MORB) (Plank and Langmuir, 1998). Subduction of these sediments, followed by extraction of Ba from the subduction slab into magmatic fluids, leads to Ba enrichment in the mantle wedge (Morris and Ryan, 2003). Thus, Ba has been used to trace subduction components in arc lavas (Elliott et al., 1997; Pearce and Stern, 2006; Plank and Langmuir, 1993, 1998) or recycled sediments in the mantle (Kuritani et al., 2011; Rapp et al., 2008).

The interest in mass-dependent Ba isotope fractionation in terrestrial (Cao et al., 2016; Horner et al., 2015; Hsieh and Henderson, 2015; Kinsley et al., 2015; Miyazaki et al., 2014; Nan et al., 2015; Pretet et al., 2016) and extraterrestrial material (Moynier et al., 2015) has

increased since the first Ba isotope study using multi-collector inductively-coupled mass spectrometry (MC-ICP-MS) (von Allmen et al., 2010). For instance, Ba isotope fractionation might take place during magmatic processes, as indicated by variable Ba isotopic compositions of igneous rocks (Miyazaki et al., 2014; Nan et al., 2015). However, the observed isotopic variability in those rocks is relatively small (<0.3 ‰ in $\delta^{137/134}$Ba; Nan et al., 2015). Larger Ba isotope fractionation is documented in low temperature environments (Pretet et al., 2016; von Allmen et al., 2010). It was found that Ba in the ocean is isotopically heterogeneous (Cao et al., 2016; Horner et al., 2015; Hsieh and Henderson, 2015; Pretet et al., 2016), and Ba isotopes may, thus, prove to be a useful indicator for different water masses with distinct isotopic compositions (Horner et al., 2015). In addition, Ba isotopes may complement the existing Ba proxies, e.g., by validating the pelagic origin of barites found in marine sediments. Yet, the fractionation mechanisms causing the observed variations in Ba isotopic composition remain largely unknown. To date, it is only established that precipitating sulphates and carbonates preferentially incorporate the lighter Ba isotopes (Böttcher et al., 2012b; von Allmen et al., 2010). From other alkali and alkaline earth metals, however, we know additional processes and reaction mechanisms that can cause isotope fractionation, such as adsorption (Bolou-Bi et al., 2010; Hindshaw et al., 2013; Huang et al., 2012), complexation (Gussone et al., 2003; Rustad et al., 2010) or diffusion (Bourg et al., 2010; Chopra et al., 2012; Richter et al., 1999; Richter et al., 2006; Watkins et al., 2009).

Our study aims to quantify the fractionation of Ba isotopes by diffusive transport through a porous, surface-reactive medium at low temperatures. In nature, such transport of dissolved Ba takes place for instance in soils, sediments and sedimentary rocks. We have designed a simplified experimental setup that will allow for diffusive transport through a silica hydrogel uniquely driven by a concentration gradient. The transport process is accompanied by sorption processes of Ba^{2+} onto reactive surface sites of the gel. Ba isotope fractionation

factors related to mass-dependent differences in the isotopes' diffusivities and the impact of Ba adsorption on the overall fractionation are evaluated using transport diffusion models. The here experimentally determined Ba isotope fractionation will provide crucial information to correctly interpret Ba isotope variations in nature.

2. MATERIALS AND METHODS

2.1. Experimental setup

Diffusion experiments were conducted in glass tubes with an inner diameter of 0.9 cm. The u-shaped glass tubes were equipped with two reservoirs for source and sink, separated by a central part containing the silica hydrogel as porous medium at a centre distance of 10 cm (Fig. 1a). Silica hydrogel was freshly prepared from sodium silicate ($Na_2SiO_3*9H_2O$) and hydrochloric acid (HCl). 13.6 g of sodium silicate were dissolved in 50 ml of de-ionized water, yielding a pH of 12.7. About 48.7 ml of the sodium silicate solution were then stepwise admixed in increasingly smaller portions with a total of 40 ml of 2 M HCl to reach a pH of 5.13. A volume of 9 ml of the still liquid medium was immediately transferred into the glass tubes where it solidified overnight. The next day, the source and sink reservoirs of the glass tubes were filled with 5 ml of $BaCl_2$ solution (pH ~7) and de-ionized water (pH ~6), respectively, and tightly closed. NaCl was formed during hydrolysis of the sodium silicate. Concentrations of NaCl in the pore fluids of the solidified gel were estimated to be about 0.86 M for all experiments. All elements were present as free ions throughout the experiment (i.e., Ba^{2+}, Na^{+} and Cl^{-}), based speciation calculations using PHREEQC (Parkhurst and Appelo, 2013).

A total of 40 single experiments were set up, divided into two separate series (G and G2), which were started within 10 months of each other. The experimental series were designed

with two defined initial Ba concentrations in the source (0.1 and 1.0 M $BaCl_2$, respectively) at two different temperatures (10 °C and 25 °C, respectively), which were kept constant using water baths. The duration of the experiments were 2, 6, 12, 20 and 27 days, respectively, for series G and 20, 40, 61, 79 and 201 days, respectively, for series G2. After the defined run duration of each experiment, source and sink solutions were sampled completely by decanting the liquids in acid-cleaned sample tubes in order to ensure homogeneity of the reservoirs. It is assumed that no significant amounts of pore fluid from the gel compartment were admixed during sampling. The sample solutions were then acidified with distilled HNO_3 to a pH of 2 and stored at 4 °C until analysis.

Isotope fractionation during adsorption of Ba onto the silica gel was determined by batch experiments. To that end, about 60 mg of solidified, aged silica gel (stored at 4°C for about 3 months) were weighed into pre-cleaned 1.5 ml centrifuge vials. 1 ml of 0.1 M and 1.0 M $BaCl_2$ stock solution, respectively, was added and the vials were gently shaken. The batch experiments were allowed to react for 67 hours at room temperature. Subsequently, the dissolved Ba in the supernatant solutions (‘ads_diss’) were separated from the gel by centrifugation and sampled by careful pipetting, avoiding contamination by gel particles. The gel was then washed twice with 1 ml MilliQ H_2O, centrifuged and the resulting wash solutions were collected for isotope analysis (‘ads_wash-I‘ and ‘ads_wash-II’). Finally, the gel was digested completely in 1 ml of a 2:1 mixture of 28 M HF and 14 M HNO_3 at 100 °C and taken to dryness. Fluorides that might have formed were subsequently dissolved in 1 ml 6.4 M HCl at 130 °C and the samples were again allowed to dry.

2.2. Sample preparation

An aliquot of each sample amounting to 1 µg of Ba was taken, mixed with an appropriate amount of ^{130}Ba-^{135}Ba double spike (von Allmen et al., 2010) and taken to dryness. Ba was

purified from the sample's matrix by cation-exchange chromatography. Custom-made Teflon columns, accommodating a 4 cm long resin bed with an inner diameter of 6 mm, were filled with 1.1 cm^3 Dowex® 50WX8 (200-400 mesh) cation-exchange resin. After cleaning (10 ml of 6.4 M HCl) and conditioning the resin (4 ml 2.5 M HCl), the samples were loaded in 0.5 ml of 2.5 M HCl. Matrix elements were eluted with additional 7.5 ml of 2.5 M HCl. Finally, Ba was collected in 5 ml of 6.4 M HCl and taken to dryness. Total procedure blanks were measured routinely over a period of 17 months, yielding an average below 0.5 ng Ba.

2.3. Analytical procedure for Ba isotope analyses

Samples were redissolved in 0.5 M HNO_3 to yield a concentration of natural Ba of 100 ppb suitable for isotope analyses. Measurements were performed on a Nu Plasma (Nu Instruments) multi-collector inductively-coupled plasma mass spectrometer (MC-ICP-MS) at the University of Bern, equipped with an ESI Apex Q sample introduction system. Signals of $^{130}Ba^+$, $^{134}Ba^+$, $^{135}Ba^+$ and $^{137}Ba^+$ were simultaneously detected together with $^{125}Te^+$ and $^{129}Xe^+$ to correct for isobaric interferences (von Allmen et al., 2010). Xe-interference contributions to ^{130}Ba and ^{134}Ba were calculated using isotope ratios published by IUPAC (de Laeter et al., 2003) that were corrected for instrumental mass bias using the exponential fractionation law. Interferences of Te were below detection limit and have been thus neglected. Data collection consisted of 10 blocks of 10 cycles with 5 s integration time. An electronic baseline (10 s integration time) was measured prior to each block. A Faraday gain calibration was performed weekly. Instrumental mass bias was corrected for by the ^{130}Ba-^{135}Ba double spike. The measured raw data were reduced using the iterative solution of Compston and Oversby (1969). However, the exponential fractionation law was used instead of the linear one.

All data are reported relative to NIST SRM 3104a using the delta-notation in per mill (‰):

$$\delta^{137/134}Ba = \left(\frac{^{137}Ba/^{134}Ba_{sample}}{^{137}Ba/^{134}Ba_{SRM3104a}} - 1\right) \cdot 1000 \quad (1)$$

The external reproducibility of sample analyses was estimated by calculating the pooled standard deviation of all repeated measurements to be ±0.09 ‰ (2 s_p) on $\delta^{137/134}$Ba. This is in excellent agreement with repeated measurements of the Fluka Aldrich $Ba(NO_3)_2$ ICP-OES standard solution used in von Allmen et al. (2010) over the course of eight months, yielding a $\delta^{137/134}$Ba value of 0.02 ± 0.09 ‰ (2 sd; n = 42).

Ba concentrations of the samples were determined by isotope dilution simultaneously with the Ba isotopic composition. For this purpose, the concentration of ^{135}Ba in the double spike was first determined by inverse isotope dilution using the NIST SRM 3104a (10.014 ± 0.036 mg g^{-1} Ba in total) to be 18.77 ± 0.18 nmol g^{-1}.

3. RESULTS

3.1. Diffusion experiments

In all experiments, the Ba concentration in the source systematically decreased with time while the Ba concentration in the sink increased (Fig. 2). The observed diffusive flux of Ba correlates positively with temperature and initial Ba concentration in the source. The monitored concentration data in source and sink of series G2 after 20 days agree well with the Ba concentration in the two reservoirs of series G after the same experimental run duration. Although two batches of silica hydrogel were separately prepared for the two experimental series, the agreement in Ba concentration after 20 days suggests that the properties of the prepared gels that influence the effective diffusivity through the gel, such as porosity and tortuosity, were comparable.

The measured $\delta^{137/134}$Ba values of the initial $BaCl_2$ solutions vary slightly within the analytical uncertainty (Table 1). For the following discussion, the isotopic compositions of

source and sink reservoirs are, thus, further expressed as $\Delta^{137/134}Ba_{sink/source}$ = $\delta^{137/134}Ba_{sink/source}$ - $\delta^{137/134}Ba_{initial}$, with $\delta^{137/134}Ba_{inital}$ corresponding to the respective initial $BaCl_2$ solution (0.1 or 1.0 M) of the experimental series G and G2. The measured Ba isotopic composition of the source of all four experimental series was indistinguishable from the initial $BaCl_2$ solution within the first 27 days, suggesting a slight increase thereafter, but still within analytical uncertainties over the experimental run time (Fig. 2). In contrast, the measured isotope ratios of the fluid from the sink reservoirs were depleted in the heavy Ba isotopes by up to -2.30 ‰ in $\Delta^{137/134}Ba_{sink}$ after 6 days (Table 1), representing the lowest $\delta^{137/134}Ba$ value measured so far (i.e., -2.15 ± 0.08 ‰). The $\Delta^{137/134}Ba$ values increased rapidly and tended towards zero with progressive run durations of the experiments. Likewise the Ba concentration data, the isotopic compositions of the source and sink reservoirs after 20 days were, within the analytical uncertainties, identical for the two series G and G2.

3.2. Batch experiment

Silica hydrogel is known to have a large, reactive surface. At pH values above the point of zero charge (PZC), which is around 3 in case of silica hydrogel (Bolt, 1957), the gel surface is negatively charged, allowing adsorption of cations. Our experiments were conducted at pH > 5, so that adsorption of Ba^{2+} onto the gel surface is expected. The batch experiments showed that adsorption of Ba onto the silica hydrogel results in significant isotope fractionation. The adsorbed Ba ('ads_gel') is enriched in the heavy Ba isotopes by 0.12 to 0.17 ‰ in $\delta^{137/134}Ba$ relative to the dissolved Ba (Table 2). The equilibrium isotope fractionation factor α can be defined as

$$\alpha = \frac{\delta^{137/134}Ba_{adsorbed}+1000}{\delta^{137/134}Ba_{dissolved}+1000} \quad (2)$$

and was accordingly calculated to be 1.00012 ± 0.00006 for 0.1 M $BaCl_2$ and 1.00017 ± 0.00002 for 1.0 M $BaCl_2$, yielding an average value of 1.00015 ± 0.00008 (2 sd). The 2 sd

uncertainties of the single experiments were determined using Monte Carlo simulations. The experimental design of the batch experiments came with the unavoidable effect that some dissolved Ba remained in the pore spaces of the gel. Therefore, two washing steps were carried out after sampling of the supernatant solution. Importantly, Ba might have been desorbed from the gel either by the washing procedure or by aging of the silica hydrogel, causing a decrease in surface area (see also section 4.1.3.). However, the isotopic compositions of Ba in the wash solutions were acidentical to that of the dissolved Ba, indicating that no significant amounts of Ba were desorbed from the gel.

The total amount of Ba adsorbed onto the silica hydrogel during the batch experiments with 0.1 M and 1.0 M $BaCl_2$ were determined to be 2.1 and 7.7 mg per ml gel, respectively. Translated to the diffusion experiments using a total of 9 ml silica hydrogel, the maximum amounts of adsorbed Ba can be estimated to be 19 and 69 mg, yielding about 29 and 10%, respectively, of the total introduced Ba.

4. DISCUSSION

4.1. Diffusive isotope effects

The migration rate of different elements or isotopes through a given medium is affected by their mass, which can result is subtle fractionation induced by the diffusive transport (Richter et al., 2003). The ratio of the effective diffusion coefficients of two isotopes D_1 and D_2 of one chemical element is related to the ratio of their molecular masses m_1 and m_2 and can be expressed as an inverse power-law function:

$$\frac{D_1}{D_2} = \left(\frac{m_2}{m_1}\right)^{\beta} \quad (3)$$

This expression is based on studies of low density gases at low pressures (i.e., virtually no interaction between single atoms or molecules) for which the relative diffusivities are simply

inversely proportional to the square root of their mass (β = 0.5). In two seminal studies, Richter et al. (2003); Richter et al. (1999) placed this concept into a geologically relevant context of diffusion in molten silicates. Melt structures are complex and, thus, the square root relation was replaced by an empirical exponent. This dimensionless exponent β can be determined either experimentally (Bourg et al., 2010; Richter et al., 2006) or by molecular dynamics (MD) simulations (Bourg et al., 2010; Bourg and Sposito, 2007). Values of β are highest (< 0.22) for elements diffusing through silicate melts (Richter et al., 2003; Richter et al., 2009; Richter et al., 2008; Watkins et al., 2009; Watkins et al., 2011) and for non-ionic species in water (Bourg and Sposito, 2008). For ions diffusing in liquid water, however, β is considerably smaller (< 0.05) (Bourg et al., 2010). The reason for this are substantial interactions of the solute with the solvent. In case of silicate melts, Si and O are strongly bound in multi-atom complexes, and a solute diffuses faster than the main matrix elements (Watkins et al., 2011). In aqueous solutions, however, water molecules are bound to diffusing ions, forming hydration shells. It has been found that β is inversely correlated with the residence time (τ_S) of water molecules in the first solvation shell (Bourg et al., 2010). τ_S is longer for divalent cations, such as Ca^{2+} and Mg^{2+}, than for monovalent ions because of a strong solute-solvent attraction interaction (Bourg et al., 2010). Therefore, alkaline earth metals show little isotope fractionation by ion diffusion in liquid water (Bourg et al., 2010; Bourg and Sposito, 2007; Richter et al., 2006).

4.1.1. Diffusive transport model

We used an implicit finite difference model in one dimension to solve simultaneously for the diffusive migration of ^{134}Ba and ^{137}Ba (denoted by i) following Fick's second law (note that all other isotopes are ignored for simplicity):

$$\frac{\partial n_i}{\partial t} = \frac{\partial}{\partial x}\left(D_i \frac{\partial n_i}{\partial x}\right) \quad (4)$$

The geometry of the model system divides the one-dimensional column into three parts comprising the sink, the silica hydrogel reservoir and the source. The spacing for the numerical calculation was set to 1 mm, resulting in 79 nodes for each the sink and the source (the length of the sink and source reservoirs equal ~7.9 cm, as determined by a volume of 5 ml solution applied in the experimental tube with an inner diameter of 0.9 cm) and 141 nodes for the length of the silica gel reservoir (corresponds to 9 ml of gel) (Fig. 1). The model system is assumed to behave as a closed system with no-flux boundaries on both ends. It allows for spatial variations of the effective diffusion coefficients in order to simulate different behaviour in the different reservoirs as will be discussed later.

Initially, the reservoirs containing the silica gel and the sink are Ba-free, while the source contains a defined number of moles of each Ba species being homogeneously distributed in the source. With time, Ba diffuses from the initially homogeneous source reservoir through the region filled with silica gel into the sink reservoir, developing the typical diffusion-type transient shape (Fig. 3a). Diffusion coefficients of ^{134}Ba were set to higher values compared with ^{137}Ba, resulting in low $\Delta^{137/134}$Ba values in sink and gel, as shown by time-resolved spatial profiles along the model geometry (Fig. 3b). At the same time, the residual source becomes enriched in the more slowly diffusing ^{137}Ba. The predicted spatial variations in isotopic composition decrease with time as the Ba concentration in the closed system homogenises, erasing the existing mass-dependent fractionation signature (Fig. 3b). Thus, subtle differences of the effective diffusion coefficients of the different isotope species lead to kinetically controlled spatial isotope fractionation according to Eq. 3.

4.1.2. Data fit

In the further discussion, the 1.0 M/10 °C diffusion experiment will be used as an example for the model fit. The three other experimental series conducted at a different temperature

and/or with a different initial $BaCl_2$ concentration are fitted comparably well by the diffusive transport model (see Supplement). Modelled Ba concentrations in sink and source were integrated over the respective reservoir at a given time, and the effective diffusion coefficients (Table 3) were determined by fitting the modelled data to the measured Ba concentrations of the sink (Fig 4d). The extracted effective diffusion coefficients were then assigned to the more abundant ^{137}Ba and the relative difference for the migration speed of ^{134}Ba was simulated by adjusting β in Eq. 3 to fit the isotopic composition measured in the sink reservoir over the experimental runtime (Fig. 4f).

The diffusive flux of the Ba species (J_i) through the silica hydrogel is affected by porosity (ϕ) and the tortuosity (τ):

$$J_i = \phi\tau D_i \frac{\partial^2 n_i}{\partial x^2} \quad (5)$$

In theory, one can determine the tortuosity of the system when both the porosity and the diffusion coefficient are well constrained and the concentration gradients are known. The porosity of the silica hydrogel used in this study was determined by drying and reweighing of a defined volume of the gel to be 0.98 ± 0.03 (2 sd). The tortuosity should be equally close to unity for such high porosities. We, therefore, do not feel confident to separate both effects for our experimental setup and treat them as factor $u = \phi * \tau$. For the present experimental setup, small deviations from unity (u = 0.95) are assumed. The overall effect of porosity and tortuosity is illustrated by adjusting the diffusive flux in the silica gel bearing reservoir using values for u from 0.5 to 1 (Fig. 5). Diffusivities in the source and sink have been held constant (with u = 1). Lower values for u, denoting a decrease in the effective diffusive flux within the silica hydrogel, do not influence the predicted evolution of Ba concentration in the sink and only slightly improve the data fit in the source (Fig. 5). However, they require higher diffusion coefficients to fit the measured Ba concentration data.

The modelled effective diffusion coefficients for u = 0.95 are comparable to published salt diffusion coefficients for $BaCl_2$ in aqueous solutions (Robinson and Stokes, 2002; Table 3). For the experiments with 1.0 M $BaCl_2$, however, they are systematically higher than published values, whereas diffusion coefficients for experiments with 0.1 M $BaCl_2$ are systematically lower, but closer to the data of Robinson and Stokes (2002) (Fig. 6). Further, the diffusion model successfully reproduces the time-dependent change in the sink phase for both the total Ba concentration (Fig. 4b) and the measured isotopic composition (Fig. 4f). However, the predicted evolution of the source reservoir does not match the measured concentrations (Fig. 4a). In all modelled scenarios (see also in the Supplement) the measured Ba concentrations systematically decrease more rapidly in the source reservoir than predicted by the simple diffusion model. This suggests a higher outflux of Ba from the source reservoir into the gel in the initial stages of the experiment.

In mixed electrolyte solutions, diffusion of an ion is affected by the electric fields generated by the other diffusing ionic species (e.g., Leaist and Curtis, 1999; Steefel and Maher, 2009). Thus, we have to consider multicomponent diffusion of $BaCl_2$ and NaCl, the latter being present in the pore fluids of the silica hydrogel with initial concentrations of about 0.8 M, with opposite concentration gradients between source and gel compartment. Multicomponent diffusion was modelled using PHREEQC (Parkhurst and Appelo, 2013), described in detail in the Supplement. The model indicates that multicomponent diffusion only affects the effective diffusivity of Ba in the 1.0 M $BaCl_2$ experiments and that it is negligible for the 0.1 M experiments. This is in agreement with the observation that the diffusion coefficients extracted from the numerical transport model for the 0.1 M $BaCl_2$ experiments are very close to the published salt diffusion coefficients of $BaCl_2$ in pure water. Furthermore, the PHEEQC simulation predicts higher effective Ba diffusivities for the 1.0 M $BaCl_2$ experiments, which is again in agreement with the higher diffusion coefficients needed

in our numerical solution to fit the measured concentrations in the sink reservoir compared to literature.

However, comparison of the spatially integrated amount of Ba in the source after 20 days (453 mg Ba) with the measured value from the 1.0 M/25 °C experiment (357 mg Ba) suggests that enhanced fluxes due to multicomponent diffusion alone is insufficient to explain the observed deviation between our numerical model and the experimental data. In addition, the multicomponent effect can only be expected to vanish when approaching complete homogenisation of the system, which is in disagreement with the convergence of the modelling results and the experimental data after 20 days while significant concentration gradients were still present. We therefore suggest that the effect of multicomponent diffusion is likely to be compensated by using a higher effective diffusion coefficient, justifying the use of a simple one-component diffusion model for the purpose of this study.

At the beginning of the diffusion experiment, differences in density existed between the $BaCl_2$ solutions in the source (1.018 and 1.171 g cm^{-1} for 0.1 M and 1.0 M $BaCl_2$, respectively, at 25 °C; Puchalska and Atkinson (1991)) and the deionised water in the sink reservoir (0.997 g cm^{-1} at 25 °C). Due to the vertical alignment of the source and sink reservoirs, these density differences were most likely compensated by a short-lived, local advective flux component from the source into the gel reservoir, resulting in a net increase of the observed effective diffusion coefficient, as demonstrated by Debacq et al. (2003). This effect could explain both the lower measured Ba concentrations in the source compared to the model and the higher effective diffusion coefficients for the 1.0 M $BaCl_2$ experiments compared to Ba salt diffusion in literature. For the 0.1 M experiments, Ba diffusivities are less affected, as the density difference is considerably smaller. In terms of transport properties, the advective flux describes the motion of medium itself, rather than its

components. Thus, fractionation of Ba isotopes should not be affected by the advective transport process.

4.1.3. Ba adsorption onto silica hydrogel

Another process affecting the transport properties and possibly fractionation of Ba is adsorption of the species on the surface of the silica gel. On the one hand, eq. 5 dictates that the diffusive flux decreases with a decreasing concentration gradient, as it would be the case of a simple continuous diffusion process. Neglecting multicomponent diffusion and advective transport, a relative enhancement of the diffusive flux can also be achieved by holding the concentration gradient close to its initial value, e.g. by a virtual removal of dissolved Ba from the fluid through adsorption on the surface of the silica gel. As shown by the batch experiment, Ba is indeed adsorbed onto the gel surface, accompanied by significant isotope fractionation. The question arises to which extent the overall Ba isotope fractionation measured in the diffusion experiments was affected by adsorption.

Therefore, the diffusive transport model was extended to include an additional fractionation process via adsorption of Ba on the surface of the silica hydrogel. A fractionation factor of α = 1.00015 was used, based on the batch experiments of this study. The maximum amount of adsorbed Ba was a fitting parameter and turned out to be variable for the four diffusion experiments (Table 3). In all cases, however, the fitted value was smaller or equal to the amounts that were experimentally determined by the batch experiments (i.e., 19 mg total Ba for 0.1 M $BaCl_2$ and 69 mg for 1.0 M $BaCl_2$ starting solution). The model assumes a linear rate to define the amount of Ba being adsorbed over time. The adsorption kinetics can be used as a fitting parameter as it controls the net flux of Ba, as, for instance, high adsorption rates can significantly decrease the net flux through the gel until saturation of the gel surface is reached, affecting both the concentration profiles in

the sink and the predicted isotope fractionation. The presented model runs have been assigned an adsorption rate that reaches saturation of the gel surface with respect to Ba after approximately 100 days, i.e., half of the total run duration. To evaluate whether adsorption kinetics have a significant effect on concentration profiles and resulting fractionation, two end-member scenarios have been modelled (not shown here), one with basically instantaneous adsorption until saturation and another with slow adsorption reaching the experimentally constrained maximum value only at the end of the experiment. It was found that modelling results of both scenarios yield concentration profiles and predicated isotope fractionation that are almost indistinguishable. In addition, no quantitative rate data are available to date despite the adsorption data derived from the batch experiments and thus using a linear rate law is a reasonable simplification for the purpose of this study.

The extended model predicts a slightly faster decrease in the source's Ba concentration (Fig. 4 a). However, the data fits, especially in the source (Fig. 4 b), do not improve. In either reservoir, the extended model fails to predict the measured concentration at t = 201 days. Enabling adsorption requires even higher diffusion coefficients (Table 3, Fig. 6) in order to fit the measured Ba concentrations in the sink. The maximum amount of adsorbed Ba calculated by the batch experiments is only a rough estimate, and the adsorption capacity of the silica hydrogel used in the diffusion experiments might deviate. Therefore, we did an additional run with 196 mg maximal adsorbed Ba, corresponding to about 30% of the total applied Ba in the 1.0 M $BaCl_2$ experiments (Fig. 4; grey dashed curves). In this case, the model greatly underestimates the Ba concentration in both the source and the sink after t = 61 days, while the diffusivities increase even further (Table 3).

The drawback of our extended model is that it does not take in account non-linear adsorption and the evolution of the silica gel surface with time. The silica hydrogel used for this study was formed by the sol-gel process, which is described in detail by Brinker and

Scherer (1990). As the gel ages with time, the specific surface area decreases, resulting in fewer surface sinalol groups on which Ba^{2+} can be adsorbed and eventually inducing desorption if sorption equilibrium is considered. Aging of silica hydrogel becomes more pronounced with increasing pH and temperature (Brinker and Scherer, 1990). In an earlier study, the specific surface area of a sodium silicate based gel, aged at room temperature under pH conditions similar to our experiments (pH ~ 6), was found to decrease by about 40 to 50% within the first 10 days after gelation (Sheinfain et al., 1965). Later it was shown that changes in surface area decelerate with time, with ~30% and ~40% decrease after 67 and 168 days, respectively (Sheinfain and Neimark, 1973). Based on these studies, changes in silica gel surface and adsorption kinetics are likely to have occurred during the course of the diffusion experiments. However, the contribution of adsorption to the overall Ba isotope fractionation is small, as will be discussed in the following paragraph.

4.1.4. Ba isotope fractionation factor

The model fits of the measured $\Delta^{137/134}$Ba data are quite sensitive to the choice of β. Based on the fits presented in Fig. 7, we estimate the uncertainty of the modelled β to be about ±0.002. Considering diffusion only, β takes values for the 0.1 M and 1.0 M experiments of 0.010 and 0.011, respectively (Table 3), which are indistinguishable within uncertainty. There is further no observed dependence on temperature. If adsorption contributed significantly to the overall Ba isotope fractionation, the model fits of the measured $\Delta^{137/134}$Ba data would become worse resulting in a required adjustment of extracted β to force the model back to the best fit. This, in turn, would allow quantitatively separate the contribution of adsorption and diffusion on the overall measured fractionation. For our experiments, however, differences in the data fits between the models with and without adsorption are minuscule, and even in case of 30% adsorption of the initially applied Ba, the measured data can still be

reasonably well fitted (Fig. 4f) with a β value of 0.011 for all experiments (Table 3). We, therefore, conclude that adsorption contributed only to a small proportion to the overall fractionation, and we can compare the diffusive Ba isotope fractionation with other aqueous systems.

For Ca, Bourg et al. (2010) experimentally determined a β of 0.0045. The residence time τ_S of water molecules in the first hydration shell of Ba is shorter than τ_S of Ca (Hofmann et al., 2013) and due to the inverse correlation of β with τ_S (Bourg et al., 2010), we can expect $\beta_{Ba} \geq \beta_{Ca}$. Further, Watkins et al. (2011) describes a systematic relationship between the diffusive isotope fractionation, denoted as $E = 2*[\ln(D_2/D_1)]/[\ln(m_1/m_2)] = 2*\beta$, of cations in water and their solvent-normalised diffusivities (i.e., D_{cation}/D_{H2O}). We tried to estimate β_{Ba} by using this relationship. At a given temperature, D_{H2O} is constant and β correlates directly with the diffusivity. We further assume that β is independent from the cation's concentration in diluted solutions. β values for Li, Na, K, Mg and Ca, either experimentally derived (Bourg et al., 2010; Richter et al., 2006) or calculated by MD simulations (Bourg et al., 2010), are plotted against the chloride salt diffusion coefficients at infinite dilution and 75 °C of the corresponding cations (Fig. 8). A linear relation can be described by $\beta = 0.0190 * D - 0.0596$ and $\beta = 0.0219 * D - 0.0681$ for experimental data and MD simulations, respectively. Accordingly, β_{Ba} values of 0.009 (experimental) and 0.011 (MD simulations) can be calculated. These values are in excellent agreement with our experimentally derived β between 0.010 and 0.011 (Table 3).

4.2. Geological implications

Following the theory of isotope fractionation (Schauble, 2004), Ba isotope effects under equilibrium conditions should be small, due to the high mass of Ba and the fact that Ba occurs in nature almost exclusively in the +2 oxidation state. Under kinetically controlled

conditions, however, Ba isotope fractionation may be substantial (Hofmann et al., 2013). Indeed, considerable variations in the Ba isotopic composition of natural barites have been found (von Allmen et al., 2010). Marine biogenic barites precipitate in the upper part of the water column in microenvironments that are created by the degradation of planktonic organic matter (see Griffith and Paytan, 2012 for review), and settle to the seafloor. There, the barite crystals can be preserved when buried in oxic sediments as long as sulphate in pore fluids remains saturated with respect to barite (Paytan and Griffith, 2007). In zones of sulphate reduction in anoxic sediments, however, barite is dissolved and Ba is released into the pore water. The dissolved Ba^{2+} is then transported upwards by advective fluid flow and/or diffusion into zones with sulphate-bearing pore waters and diagenetic barite precipitates (Torres et al., 1996). Biogenic barite that forms in the water column has $\delta^{137/134}$Ba values of around 0 ‰ (Böttcher et al., 2012a). Diagenetic barite from the Demerara Rise, on the other hand, was found to be enriched in the light Ba isotopes with a $\delta^{137/134}$Ba value of around -0.5 ‰ (von Allmen et al., 2010). von Allmen et al. (2010) suggested ion diffusion, sorption processes and/or precipitation as possible reasons for the observed differences in Ba isotopic composition of the barites. Indeed, precipitation enriches barite in the lighter Ba isotopes by about -0.25 ‰ (von Allmen et al., 2010). The here presented results suggest that, next to precipitation, diffusive transport (with or without accompanying adsorption) may also contribute significantly to the fractionated Ba isotopic composition of diagenetic barites, as upwardly diffusing Ba^{2+} in pore waters may become isotopically lighter. The contribution of adsorption on the overall isotope fractionation is likely to be variable for different substrates. Moreover, the direction and magnitude of isotope fractionation during adsorption, in absence of redox changes, is in general controlled by changes in complexation and coordination of the element in solution and at the particle surface (e.g., Jiskra et al., 2012; Juillot et al., 2008; Kafantaris and Borrok, 2014; Mulholland et al., 2015; Siebert et al., 2003; Wasylenki et al.,

2011). Therefore, isotope effects caused by adsorption of Ba on organic and mineral particles in marine sediments may differ from here determined fractionation for silica hydrogel under laboratory conditions.

As outlined above, first results indicate that Ba isotopes are substantially fractionated in marine sediments. The abundance of organic and mineral Ba-bearing particles as well as their Ba isotopic composition might be highly variable, depending on the composition of the sediment and the extent of processes responsible for isotope fractionation, such as $BaSO_4$ precipitation after sulphate reduction as well as adsorption and diffusion of Ba^{2+} ions. Furthermore, it is very likely that a number of other (bio)chemical reactions can cause significant Ba isotope fractionation as well. Thus, marine sediments might not be isotopically homogenous on a regional to global scale. This, in turn, might prove to be an important aspect of using Ba isotopes as tracers of subducted sediments, as proposed by Miyazaki et al. (2014) and Nan et al. (2015).

5. CONCLUSIONS

Our experiments show that diffusion of dissolved Ba^{2+} ions through a permeable substrate may result in considerable Ba isotope fractionation. Despite rather small fractionation factors, measured $\delta^{137/134}$Ba values exceeded those of former studies by up to one order of magnitude. Diffusive transport and isotope fractionation could be adequately retraced by a numerical transport model. Diffusion of Ba through a silica hydrogel was likely affected by an initial, short-lived advective flux of $BaCl_2$ solution into the silica gel due to density differences of the solutions in the system, multicomponent diffusion in the system $BaCl_2$-NaCl-H_2O and adsorption of Ba onto the gel surface. Multicomponent diffusion and gravitational mixing have presumably negligible effects on diffusive isotope fractionation studied here. In other

(natural) systems, however, multicomponent diffusion and advection are likely to influence other parameters such as pH and adsorption capacities, and it is therefore desirable to incorporate these effects in future models.

Isotope fractionation during the diffusion experiments is related to subtle mass-dependent differences in the effective diffusivities of the isotopes ($D \propto m^{-\beta}$), with β factors between 0.010 and 0.011 for Ba diffusion. Adsorption of Ba onto the silica hydrogel surface was accompanied by isotope fractionation with $\alpha = 1.00015 \pm 0.00008$, determined by batch experiments. The contribution of adsorption to the overall Ba isotope fractionation in our diffusion experiments was evaluated by extending the numerical transport model by a linear adsorption term. Adsorption was subsequently found to have a small impact on the observed Ba isotope fractionation. As diffusion is a pervasive process in nature, the results of our study indicate that considerable transport-driven Ba isotope fractionation can be expected, especially in a highly permeable and surface-reactive substrate such as marine sediments.

Acknowledgements

We thank Maria Hierz and Andrea Wolf from the TU Graz for laboratory support with preparation of silica hydrogel and conduction of the diffusion experiments. Jennifer Druhan and two anonymous reviewers are thanked for constructive comments that greatly improved the quality of the manuscript. This work was supported by the Swiss National Science Foundation (SNSF Grant 200021_140223 to TFN). The paper is a contribution to the collaborative research initiative CHARON, financed by the German Research Foundation.

Appendix A. Supplementary data

Supplementary data to this article can be found online at xxx

References

Bishop, J.K.B., 1988. The barite-opal-organic carbon association in oceanic particulate matter. Nature 332, 341-343.

Bolou-Bi, E.B., Poszwa, A., Leyval, C., Vigier, N., 2010. Experimental determination of magnesium isotope fractionation during higher plant growth. Geochim. Cosmochim. Acta 74, 2523-2537.

Bolt, G.H., 1957. Determination of the charge density of silica sols. J. Phys. Chem. A 61, 1166-1169.

Böttcher, M., van Allmen, K., Paytan, A., Neubert, N., Brumsack, H.J., Samankassou, E., Nägler, T.F., 2012a. A new look on the barium cycle: Stable barium isotope fractionation in ODP sediments and calibration experiments. Mineral. Mag. 76, 1495.

Böttcher, M.E., Geprägs, P., Neubert, N., Von Allmen, K., Pretet, C., Samankassou, E., Nägler, T.F., 2012b. Barium isotope fractionation during experimental formation of the double carbonate $BaMn[CO_3]_2$ at ambient temperature. Isot. Environ. Healt. S. 48, 457-463.

Bourg, I.C., Richter, F.M., Christensen, J.N., Sposito, G., 2010. Isotopic mass dependence of metal cation diffusion coefficients in liquid water. Geochim. Cosmochim. Acta 74, 2249-2256.

Bourg, I.C., Sposito, G., 2007. Molecular dynamics simulations of kinetic isotope fractionation during the diffusion of ionic species in liquid water. Geochim. Cosmochim. Acta 71, 5583-5589.

Bourg, I.C., Sposito, G., 2008. Isotopic fractionation of noble gases by diffusion in liquid water: Molecular dynamics simulations and hydrologic applications. Geochim. Cosmochim. Acta 72, 2237-2247.

Brinker, C.J., Scherer, G.W., 1990. Sol-Gel Science: The Physics and Chemistry of Sol-Gel Processing. Academic Press, Boston.

Cao, Z., Siebert, C., Hathorne, E.C., Dai, M., Frank, M., 2016. Constraining the oceanic barium cycle with stable barium isotopes. Earth Planet. Sc. Lett. 434, 1-9.

Chopra, R., Richter, F.M., Watson, E.B., Scullard, C.R., 2012. Magnesium isotope fractionation by chemical diffusion in natural settings and in laboratory analogues. Geochim. Cosmochim. Acta 88, 1-18.

Compston, W., Oversby, V.M., 1969. Lead Isotopic Analysis Using a Double Spike. J. Geophys. Res. 74, 4338-4348.

Cronan, D.S., Hodkinson, R.A., 1997. Geochemistry of hydrothermal sediments from ODP sites 834 and 835 in the Lau Basin, southwest Pacific. Mar. Geol. 141, 237-268.

de Laeter, J.R., Böhlke, J.K., De Bièvre, P., Hidaka, H., Peiser, H.S., Rosman, K.J.R., Taylor, P.D.P., 2003. Atomic weights of the elements: Review 2000 (IUPAC Technical report). Puer Appl. Chem. 75, 683-800.

Debacq, M., Hulin, J.-P., Salin, D., Perrin, B., Hinch, E.J., 2003. Buoyant mixing of miscible fluids of varying viscosities in vertical tubes. Phys. Fluids 15, 3846-3855.

Dehairs, F., Chesselet, R., Jedwab, J., 1980. Discrete suspended particles of barite and the barium cycle in the open ocean. Earth Planet. Sc. Lett. 49, 528-550.

Dymond, J., Collier, R., 1996. Particulate barium fluxes and their relationships to biological productivity. Deep-Sea Res. Pt. II 43, 1283-1308.

Dymond, J., Suess, E., Lyle, M., 1992. Barium in deep-sea sediment: A geochemical proxy for paleoproductivity. Paleoceanography 7, 163-181.

Elliott, T., Plank, T., Zindler, A., White, W., Bourdon, B., 1997. Element transport from slab to volcanic front at the Mariana arc. J. Geophys. Res. 102, 14991-15019.

François, R., Honjo, S., Manganini, S.J., Ravizza, G.E., 1995. Biogenic barium fluxes to the deep sea: Implications for paleoproductivity reconstruction. Global Biogeochem. Cy. 9, 289-303.

Ganeshram, R.S., François, R., Commeau, J., Brown-Leger, S.L., 2003. An experimental investigation of barite formation in seawater. Geochim. Cosmochim. Acta 67, 2599-2605.

Goldberg, E.D., Arrhenius, G.O.S., 1958. Chemistry of Pacific pelagic sediments. Geochim. Cosmochim. Acta 13, 153-198.
Griffith, E.M., Paytan, A., 2012. Barite in the ocean – occurrence, geochemistry and palaeoceanographic applications. Sedimentology 59, 1817-1835.
Gussone, N., Eisenhauer, A., Heuser, A., Dietzel, M., Bock, B., Böhm, F., Spero, H., Lea, D.W., Bijma, J., Nägler, T.F., 2003. Model for kinetic effects on calcium isotope fractionation ($\delta^{44}Ca$) in inorganic aragonite and cultured planktonic foraminifera. Geochim. Cosmochim. Acta 67, 1375-1382.
Hindshaw, R.S., Reynolds, B.C., Wiederhold, J.G., Kiczka, M., Kretzschmar, R., Bourdon, B., 2013. Calcium isotope fractionation in alpine plants. Biogeochemistry 112, 373-388.
Hofmann, A.E., Bourg, I.C., DePaolo, D.J., 2013. Ion desolvation as a mechanism for kinetic isotope fractionation in aqueous systems. PNAS 109, 18689-18694.
Horner, T.J., Kinsley, C.W., Nielsen, S.G., 2015. Barium-isotopic fractionation in seawater mediated by barite cycling and oceanic circulation. Earth Planet. Sc. Lett. 430, 511-522.
Hsieh, Y.-T., Henderson, G.M., 2015. Barium stable isotope fractionation in seawater, Goldschmidt Abstracts, p. 1326.
Huang, K.-J., Teng, F.-Z., Wei, G.-J., Ma, J.-L., Bao, Z.-Y., 2012. Adsorption- and desorption-controlled magnesium isotope fractionation during extreme weathering of basalt in Hainan Island,China. Earth Planet. Sc. Lett. 359-360, 73-83.
Hull, P.M., Norris, R.D., 2011. Diverse patterns of ocean export productivity change across the Cretaceous-Paleogene boundary: New insights from biogenic barium. Paleoceanography 26, PA3205.
Jiskra, M., Wiederhold, J.G., Bourdon, B., Kretzschmar, R., 2012. Solution Speciation Controls Mercury Isotope Fractionation of Hg(II) Sorption to Goethite. Environ. Sci. Technol. 46, 6654-6662.
Juillot, F., Maréchal, C., Ponthieu, M., Cacaly, S., Morin, G., Benedetti, M., Hazemann, J.L., Proux, O., Guyot, F., 2008. Zn isotopic fractionation caused by sorption on goethite and 2-Lines ferrihydrite. Geochim. Cosmochim. Acta 72, 4886-4900.
Kafantaris, F.-C.A., Borrok, D.M., 2014. Zinc isotope fractionation during surface adsorption and intracellular incorporation by bacteria. Chem. Geol. 366, 42-51.
Kinsley, C.W., Horner, T.J., Nielsen, S.G., Lam, P.J., 2015. Barium-isotopic cycling in Southern Ocean particulate matter, Goldschmidt Abstracts, p. 1596.
Kuritani, T., Ohtani, E., Kimura, J.-I., 2011. Intensive hydration of the mantle transition zone beneath China caused by ancient slab stagnation. Nat. Geosci. 4, 713-716.
Leaist, D.G., Curtis, N., 1999. Hartley-Crank equations for coupled diffusion in concentrated mixed electrolyte solutions. The
$CaCl_2 + HCl + H_2O$ system. J. Solution Chem. 28, 341-366.
Li, Y.-H., Gregory, S., 1974. Diffusion of ions in sea water and in deep-sea sediments. Geochim. Cosmochim. Acta 88, 708-714.
McManus, J., Berelson, W.M., Klinkhammer, G.P., Johnson, K.S., Coale, K.H., Anderson, R.F., Kumar, N., Burdige, D.J., Hammond, D.E., Brumsack, H.J., McCorkle, D.C., Rushdi, A., 1998. Geochemistry of barium in marine sediments: Implications for its use as a paleoproxy. Geochim. Cosmochim. Acta 62, 3453-3473.
Miyazaki, T., Kimura, J.-I., Chang, Q., 2014. Analysis of stable isotope ratios of Ba by double-spike standard-bracketing using multiple-collector inductively coupled plasma mass spectrometry. J. Anal. Atom. Spectrom. 29, 483-490.
Morris, J.D., Ryan, J.G., 2003. Subduction zone processes and implications for changing composition of the upper and lower mantle, Treatise on geochemistry, pp. 451-470.
Moynier, F., Pringle, E.A., Bouvier, A., Moureau, J., 2015. Barium stable isotope composition of the Earth, meteorites, and calcium–aluminum-rich inclusions. Chem. Geol. 413, 1-6.

Mulholland, D.S., Poitrasson, F., Shirokova, L.S., González, A.G., Pokrovsky, O.S., Boaventura, G.R., Vieira, L.C., 2015. Iron isotope fractionation during Fe(II) and Fe(III) adsorption on cyanobacteria. Chem. Geol. 400, 24-33.
Nan, X., Wu, F., Zhang, Z., Hou, Z., Huang, F., Yu, H., 2015. High-precision barium isotope measurement by MC-ICP-MS. J. Anal. Atom. Spectrom., DOI: 10.1039/C1035JA00166H.
Parkhurst, D.L., Appelo, C.A.J., 2013. Description of input and examples for PHREEQC version 3: a computer program for speciation, batch-reaction, one-dimensional transport, and inverse geochemical calculations, Modeling Techniques. U.S. Geological Survey, Reston, VA, p. A43.
Paytan, A., Averyt, K., Faul, K., Gray, E., Thomas, E., 2007. Barite accumulation, ocean productivity, and Sr/Ba in barite across the Paleocene–Eocene Thermal Maximum. Geology 35, 1139-1142.
Paytan, A., Griffith, E.M., 2007. Marine barite: Recorder of variations in ocean export productivity. Deep-Sea Res. Pt. II 54, 687-705.
Paytan, A., Kastner, M., 1996. Benthic Ba fluxes in the central Equatorial Pacific, implications for the oceanic Ba cycle. Earth Planet. Sc. Lett. 142, 439-450.
Pearce, J.A., Stern, R.J., 2006. Origin of back-arc basin magmas: Trace element and isotope perspectives, in: Christie, D.M., Fisher, C.R., Sang-Mook, L., Givens, S. (Eds.), Back-arc spreading systems: Geological, biological, chemical, and physical interactions. American Geophysical Union, Washington DC, pp. 63-86.
Plank, T., Langmuir, C.H., 1993. Tracing trace elements from sediment input to volcanic output at subduction zones. Nature 362, 739-743.
Plank, T., Langmuir, C.H., 1998. The chemical composition of subducting sediment and its consequences for the crust and mantle. Chem. Geol. 145, 325-394.
Pretet, C., van Zuilen, K., Nägler, T.F., Reynaud, S., Böttcher, M.E., Samankassou, E., 2016. Constraints on barium isotope fractionation during aragonite precipitation by corals. The Depositional Record 1, 118-129.
Puchalska, D., Atkinson, G., 1991. Densities and apparent molal volumes of aqueous $BaCl_2$ solutions from 15 to 140 °C and from 1 to 200 bar. J. Chem. Eng. Data 36, 449-452.
Rapp, R.P., Irifune, T., Shimizu, N., Nishiyama, N., Norman, M.D., Inoue, T., 2008. Subduction recycling of continental sediments and the origin of geochemically enriched reservoirs in the deep mantle. Earth Planet. Sc. Lett. 271, 14-23.
Richter, F.M., Davis, A.M., DePaolo, D.J., Watson, E.B., 2003. Isotope fractionation by chemical diffusion between molten basalt and rhyolite. Geochim. Cosmochim. Acta 67, 3905-3923.
Richter, F.M., Liang, Y., Davis, A.M., 1999. Isotope fractionation by diffusion in molten oxides. Geochim. Cosmochim. Acta 63, 2853-2861.
Richter, F.M., Mendybaev, R.A., Christensen, J.N., Hutcheon, I.D., Williams, R.W., Sturchio, N.C., Beloso Jr., A.D., 2006. Kinetic isotopic fractionation during diffusion of ionic species in water. Geochim. Cosmochim. Acta 70, 277-289.
Richter, F.M., Watson, E.B., Mendybaev, R.A., Dauphas, N., Georg, B., Watkins, J., Valley, J., 2009. Isotopic fractionation of the major elements of molten basalt by chemical and thermal diffusion. Geochim. Cosmochim. Acta 73, 4250-4263.
Richter, F.M., Watson, E.B., Mendybaev, R.A., Teng, F.-Z., Janney, P.E., 2008. Magnesium isotope fractionation in silicate melts by chemical and thermal diffusion. Geochim. Cosmochim. Acta 72, 206-220.
Robinson, R.A., Stokes, R.H., 2002. Electrolyte solutions. Dover Publications, Mineola, NY.
Rustad, J.R., Casey, W.H., Yin, Q.-Z., Bylaska, E.J., Felmy, A.R., Bogatko, S.A., Jackson, V.E., Dixon, D.A., 2010. Isotopic fractionation of Mg^{2+}(aq), Ca^{2+}(aq), and Fe^{2+}(aq) with carbonate minerals. Geochim. Cosmochim. Acta 74, 6301-6323.
Schauble, E.A., 2004. Applying Stable Isotope Fractionation Theory to New Systems, in: Johnson, C.M., Beard, B.L., Albarède, F. (Eds.), Geochemistry of Non-Traditional Stable Isotopes. Mineralogical Society of America, Washington, pp. 65-111.

Sheinfain, R.Y., Neimark, I.E., 1973. Role of the ageing of silicic acid hydrogel in the formation of the porous structure of silica gel, in: Strazhesko, D.N. (Ed.), Adsorption and Adsorbents. John Wiley & Sons, New York, pp. 87-95.
Sheinfain, R.Y., Stas, O.P., Neimark, I.E., 1965. Mechanism of porous structure formation of silica gels. IV. Regulation of silica structure by combination of variation of gel aging time and the nature of intermicellar liquid. Colloid J. USSR 27, 781-784.
Siebert, C., Nägler, T.F., von Blanckenburg, F., Kramers, J.D., 2003. Molybdenum isotope records as a potential new proxy for paleoceanography. Earth Planet. Sc. Lett. 211, 159-171.
Steefel, C.I., Maher, K., 2009. Fluid-rock interaction: a reactive transport approach, in: Oelkers, E.H., Schott, J. (Eds.), Thermodynamics and kinetics of water-rock interaction. Mineralogical Society of America, Washington, pp. 485-532.
Torres, M.E., Brumsack, H.J., Bohrmann, G., Emeis, K.C., 1996. Barite fronts in continental margin sediments: A new look at barium remobilization in the zone of sulfate reduction and formation of heavy barites in diagenetic fronts. Chem. Geol. 127.
von Allmen, K., Böttcher, M.E., Samankassou, E., Nägler, T.F., 2010. Barium isotope fractionation in the global barium cycle: First evidence from barium minerals and precipitation experiments. Chem. Geol. 277, 70-77.
Wasylenki, L.E., Weeks, C.L., Bargar, J.R., Spiro, T.G., Hein, J.R., Anbar, A.D., 2011. The molecular mechanism of Mo isotope fractionation during adsorption to birnessite. Geochim. Cosmochim. Acta 75, 5019-5031.
Watkins, J.M., DePaolo, D.J., Huber, C., Ryerson, F.J., 2009. Liquid composition-dependence of calcium isotope fractionation during diffusion in molten silicates. Geochim. Cosmochim. Acta 73, 7341-7359.
Watkins, J.M., DePaolo, D.J., Ryerson, F.J., Peterson, B.T., 2011. Influence of liquid structure on diffusive isotope separation in molten silicates and aqueous solutions. Geochim. Cosmochim. Acta 75, 3103-3118.

Tables

Table 1

Ba concentration and isotope data of diffusion experiments

sample ID	time (days)	Ba (µg/g)	2 sd	$\delta^{137/134}$Ba repl 1	$\delta^{137/134}$Ba repl 2	$\delta^{137/134}$Ba average	$\delta^{137/134}$Ba 2 sd		$\Delta^{137/134}$Ba [a]
Initial solutions									
G_0.1M_BaCl2	0	13313.62	245.86	0.07	0.05	0.06	0.03		n/a
G2_0.1M_BaCl2	0	13046.19	285.10	0.06	0.08	0.07	0.04		n/a
G_1.0M_BaCl2	0	132739.70	2814.34	0.17	0.12	0.15	0.07		n/a
G2_1.0M_BaCl2	0	129792.06	2929.35	0.01	0.01	0.01	0.00		n/a
Sink									
G_0.1_10_2d_H2O	2	0.01	0.00			n/d			
G_0.1_10_6d_H2O	6	0.01	0.00			n/d			
G_0.1_10_12d_H2O	12	0.48	0.00	-0.95	-0.93	-0.94	0.02		-1.00
G_0.1_10_20d_H2O	20	5.16	0.07	-1.01	-1.01	-1.01	0.01		-1.07
G_0.1_10_27d_H2O	27	24.27	0.34	-0.78	-0.80	-0.79	0.02		-0.85
G2_0.1_10_20d_H2O	20	6.16	0.08	-0.94	-0.96	-0.95	0.02		-1.02
G2_0.1_10_40d_H2O	40	83.21	2.53	-0.86	-0.83	-0.84	0.04		-0.91
G2_0.1_10_61d_H2O	61	260.39	3.93	-0.53	-0.56	-0.54	0.04		-0.61
G2_0.1_10_79d_H2O	79	522.44	10.02	-0.40	-0.38	-0.39	0.03		-0.46
G2_0.1_10_201d_H2O	201	2103.66	43.53	-0.15	-0.11	-0.13	0.06		-0.20
G_0.1_25_2d_H20	2	0.01	0.00			n/d			
G_0.1_25_6d_H2O	6	0.20	0.00	-1.61	-	-1.61	0.09	[b]	-1.67
G_0.1_25_12d_H2O	12	4.03	0.11	-1.10	-1.10	-1.10	0.00		-1.16
G_0.1_25_20d_H2O	20	37.04	0.87	-0.67	-0.81	-0.74	0.20		-0.80
G_0.1_25_27d_H2O	27	125.32	1.93	-0.49	-0.66	-0.57	0.24		-0.63
G2_0.1_25_20d_H2O	20	25.65	0.50	-0.87	-0.89	-0.88	0.04		-0.95
G2_0.1_25_40d_H2O	40	269.70	5.29	-0.56	-0.58	-0.57	0.02		-0.64
G2_0.1_25_61d_H2O	61	750.25	14.13	-0.42	-0.44	-0.43	0.03		-0.50
G2_0.1_25_79d_H2O	79	1069.68	19.80	-0.28	-0.32	-0.30	0.07		-0.37
G2_0.1_25_201d_H2O	201	2794.34	65.82	-0.01	-0.03	-0.02	0.03		-0.09
G_1.0_10_2d_H2O	2	0.01	0.00			n/d			
G_1.0_10_6d_H2O	6	0.03	0.00	-2.15	-	-2.15	0.09	[b]	-2.30
G_1.0_10_12d_H2O	12	8.93	0.11	-1.58	-1.53	-1.55	0.08		-1.70
G_1.0_10_20d_H2O	20	153.90	2.59	-0.94	-0.97	-0.96	0.04		-1.10
G_1.0_10_27d_H2O	27	783.16	13.35	-0.62	-0.65	-0.63	0.04		-0.78
G2_1.0_10_20d_H2O	20	186.47	3.40	-0.95	-0.92	-0.93	0.05		-0.95
G2_1.0_10_40d_H2O	40	2091.39	41.03	-0.69	-0.73	-0.71	0.06		-0.72
G2_1.0_10_61d_H2O	61	5415.34	152.30	-0.45	-0.49	-0.47	0.06		-0.48
G2_1.0_10_79d_H2O	79	8700.28	167.56	-0.35	-0.41	-0.38	0.07		-0.39
G2_1.0_10_201d_H2O	201	25194.84	601.88	-0.05	-0.09	-0.07	0.07		-0.08
G_1.0_25_2d_H2O	2	0.01	0.00			n/d			

G_1.0_25_6d_H2O	6	1.12	0.03	-2.06	-1.99	-2.02	0.10	-2.17
G_1.0_25_12d_H2O	12	113.18	1.69	-1.02	-1.11	-1.07	0.13	-1.21
G_1.0_25_20d_H2O	20	904.27	15.76	-0.79	-0.91	-0.85	0.16	-1.00
G_1.0_25_27d_H2O	27	2377.26	42.77	-0.55	-0.58	-0.57	0.05	-0.72
G2_1.0_25_20d_H2O	20	605.00	10.85	-0.84	-0.79	-0.81	0.08	-0.83
G2_1.0_25_40d_H2O	40	4580.39	127.02	-0.67	-0.64	-0.65	0.04	-0.67
G2_1.0_25_61d_H2O	61	10393.99	203.85	-0.32	-0.32	-0.32	0.00	-0.33
G2_1.0_25_79d_H2O	79	14613.10	301.89	-0.25	-0.26	-0.25	0.01	-0.27
G2_1.0_25_201d_H2O	201	33860.44	876.90	-0.06	-0.03	-0.05	0.05	-0.06
Source								
G_0.1_10_2d_BaCl2	2	11863.58	228.16	0.09	0.17	0.13	0.11	0.07
G_0.1_10_6d_BaCl2	6	10987.73	208.19	0.07	0.13	0.10	0.09	0.04
G_0.1_10_12d_BaCl2	12	10223.27	191.05	0.11	0.12	0.11	0.01	0.06
G_0.1_10_20d_BaCl2	20	9404.73	176.00	0.11	0.15	0.13	0.07	0.07
G_0.1_10_27d_BaCl2	27	8449.72	156.09	0.10	0.09	0.10	0.02	0.04
G2_0.1_10_20d_BaCl2	20	9391.66	184.00	0.07	0.09	0.08	0.04	0.01
G2_0.1_10_40d_BaCl2	40	7492.29	144.46	0.10	0.12	0.11	0.03	0.04
G2_0.1_10_61d_BaCl2	61	6936.08	132.99	0.08	0.05	0.06	0.04	0.00
G2_0.1_10_79d_BaCl2	79	6306.69	120.68	0.09	0.05	0.07	0.06	0.00
G2_0.1_10_201d_BaCl2	201	4588.57	87.47	0.23	0.30	0.27	0.10	0.20
G_0.1_25_2d_H20	2	11412.24	217.37	0.10	0.08	0.09	0.03	0.03
G_0.1_25_6d_BaCl2	6	10387.94	195.61	0.12	0.12	0.12	0.00	0.06
G_0.1_25_12d_BaCl2	12	9045.05	167.64	0.13	0.10	0.12	0.05	0.06
G_0.1_25_20d_BaCl2	20	7999.65	148.09	0.10	0.20	0.15	0.14	0.09
G_0.1_25_27d_BaCl2	27	7053.36	128.93	0.10	0.21	0.15	0.16	0.10
G2_0.1_25_20d_BaCl2	20	8100.13	157.52	0.12	0.07	0.10	0.07	0.03
G2_0.1_25_40d_BaCl2	40	6535.57	125.26	0.08	0.02	0.05	0.08	-0.01
G2_0.1_25_61d_BaCl2	61	5957.27	113.70	0.10	0.10	0.10	0.00	0.03
G2_0.1_25_79d_BaCl2	79	5656.31	108.28	0.13	0.13	0.13	0.01	0.06
G2_0.1_25_201d_BaCl2	201	4066.29	92.18	0.13	0.14	0.13	0.01	0.06
G_1.0_10_2d_BaCl2	2	111520.15	2396.75	0.10	0.08	0.09	0.03	-0.06
G_1.0_10_6d_BaCl2	6	90157.33	1913.00	0.11	0.14	0.13	0.04	-0.02
G_1.0_10_12d_BaCl2	12	81450.73	1719.97	0.09	0.19	0.14	0.14	-0.01
G_1.0_10_20d_BaCl2	20	75427.74	1588.89	0.01	0.25	0.13	0.35	-0.02
G_1.0_10_27d_BaCl2	27	71369.53	1496.37	0.12	0.13	0.13	0.02	-0.02
G2_1.0_10_20d_BaCl2	20	71464.99	1561.95	0.06	0.07	0.07	0.01	0.05
G2_1.0_10_40d_BaCl2	40	63514.11	1382.80	0.12	0.06	0.09	0.09	0.08
G2_1.0_10_61d_BaCl2	61	60185.67	1309.57	0.13	0.09	0.11	0.06	0.10
G2_1.0_10_79d_BaCl2	79	56591.84	1230.29	0.04	0.11	0.08	0.09	0.06
G2_1.0_10_201d_BaCl2	201	43533.48	1401.46	0.16	0.19	0.18	0.04	0.16
G_1.0_25_2d_BaCl2	2	101318.17	2164.67	0.13	0.17	0.15	0.05	0.00
G_1.0_25_6d_BaCl2	6	83799.31	1782.31	0.12	0.19	0.15	0.10	0.01
G_1.0_25_12d_BaCl2	12	78478.81	1652.89	0.15	0.09	0.12	0.08	-0.03
G_1.0_25_20d_BaCl2	20	71370.72	1504.19	0.14	0.16	0.15	0.03	0.00

G_1.0_25_27d_BaCl2	27	66892.50	1399.71	0.10	0.17	0.13	0.10	-0.01
G2_1.0_25_20d_BaCl2	20	68527.34	1496.57	0.05	0.09	0.07	0.05	0.06
G2_1.0_25_40d_BaCl2	40	60062.35	1306.17	0.12	0.07	0.10	0.07	0.09
G2_1.0_25_61d_BaCl2	61	53541.41	1163.12	0.17	0.11	0.14	0.08	0.12
G2_1.0_25_79d_BaCl2	79	48871.50	1254.70	0.09	0.24	0.16	0.21	0.15
G2_1.0_25_201d_BaCl2	201	41403.98	1332.55	0.16	0.13	0.14	0.05	0.13

[a] isotopic composition relative to the starting solution

[b] external reproducibility $2s_p$ (see main text)

743

744

Table 2

Ba isotope data of batch equilibrium experiment

sample ID	gel (g)	gel (ml)	Ba (µg/g)	2 sd	$\delta^{137/134}$Ba repl 1	repl 2	average	2 sd		$\Delta^{137/134}$Ba [a]
0.1 M $BaCl_2$										
ads_diss			12188	498	0.11	0.07	0.09	0.05		n/a
ads_wash-I			767	17	0.05	-	0.05	0.09	[b]	-0.03
ads_wash-II			187	4	0.08	-	0.08	0.09	[b]	-0.01
ads_gel	0.0473	0.0436	91	1	0.22	0.20	0.21	0.03		0.12
1.0 M $BaCl_2$										
ads_diss			125229	5208	0.05	0.05	0.05	0.00		n/a
ads_wash-I			5925	141	0.05	-	0.05	0.09	[b]	0.00
ads_wash-II			1247	54	0.08	-	0.08	0.09	[b]	0.03
ads_gel	0.0572	0.0528	404	15	0.23	0.22	0.23	0.02		0.17

[a] isotopic composition relative to 'ads_diss'

[b] external reproducibility $2s_p$ (see main text)

745

Table 3

Parameters extracted from the diffusive transport model (with u = 0.95)

experiment	diffusion only		with adsorption			salt diffusion [a]
	D^{eff} (10^{-5} cm² s^{-1})	β	D^{eff} (10^{-5} cm² s^{-1})	β	Ba adsorbed (mg)	D (10^{-5} cm² s^{-1})
0.1 M/10 ℃	0.73	0.010	0.80	0.011	3.2	0.75
0.1 M/25 ℃	1.10	0.010	1.20	0.011	3.2	1.16
1.0 M/10 ℃	0.98	0.011	1.10	0.011	68.5	0.76
			1.40 [b]	0.011 [b]	196.0 [b]	
1.0 M/25 ℃	1.40	0.011	1.50	0.011	12.2	1.18

[a] salt diffusion coefficients for 0.1 and 1.0 M at 25 ℃ were taken from Robinson and Stokes (2002); diffusion coefficients at 10 ℃ were calculated using the Stokes-Einstein equation

[b] model run with 30% adsorption

746

Figure captions

Fig. 1. (a) Experimental setup of diffusion experiments. The bottom of the glass tube was filled with silica hydrogel. Source and sink reservoirs were filled with $BaCl_2$ solution and deionized water, respectively. (b) The solidified gel consisted of a silica network with a porosity of about 0.98. The pores were initially filled with a ~0.8 M NaCl solution as the result of the sol-gel process.

Fig. 2. Concentration data (blue) and Ba isotopic composition (black) of all four diffusion experiments plotted against time. Development of the source and sink is shown on the left (a, c, e, f) and on the right hand side (b, d, f, h), respectively. The experiments were conducted in two separate series (G and G2), with an overlap at t = 20 days. Data points are connected by straight lines for clarity only. Individual analytical uncertainties (2 sd), based on 2 repeated measurements, are indicated by the error bars, which may be smaller than symbol size. $\Delta^{137/134}$Ba of the initial $BaCl_2$ solution is 0 ‰ by default, 2 sd uncertainty is shown by grey bar.

Fig. 3. Diffusive transport model. See text for details. (a) Spatial distribution of ^{134}Ba (grey) and ^{137}Ba (black) (given in 10^{-5} mol per mm) at the beginning (solid lines) and end (dashed lines) of the experiment. At t = 0 days, the source has a homogenous Ba concentration, gel and sink reservoirs do not contain Ba. Diffusion and isotope fractionation were exemplarily modelled for the 1.0 M/10 °C experiment with an effective diffusion coefficient D^{eff} of $0.98*10^{-5}$ cm^2 s^{-1} for ^{137}Ba and a β value of 0.011. (b) Ba isotopic composition relative to the initial $BaCl_2$ solution. The sink reservoir becomes enriched in ^{134}Ba as the result of faster

771 diffusion of the lighter Ba isotopes. Subsequently, the source reservoir becomes isotopically
772 heavier with time.
773
774 Fig. 4. Fit of experimental concentration and isotope data of the 1.0 M/10 °C diffusion
775 experiment with the diffusive transport model with u = 0.95 with time. Measured and
776 modelled data of the source reservoir are shown on the left hand side, data of the sink on the
777 right hand side. 2 sd uncertainties of concentration data are smaller than symbol size. Three
778 scenarios were modelled: (1) diffusion without adsorption (solid lines), (2) diffusion plus
779 linear adsorption of maximum 5.6×10^{-5} moles ^{137}Ba and saturation of the gel surface after
780 about 100 days (blue dashed lines), (3) and diffusion plus adsorption of 1.6×10^{-4} moles ^{137}Ba
781 (grey dashed lines). The total Ba concentration (b) and the concentration of ^{134}Ba and ^{137}Ba
782 (d) in the sink reservoir are fitted well when neglecting adsorption. Allowing adsorption, the
783 model underestimates the Ba concentrations in the sink. The concentrations in the source
784 reservoir (a, c) are overestimated by the diffusion model for $t \leq 80$ days for scenarios (1) and
785 (2). In scenario (3) data fit can be improved for the first 40 days, whilst data for $t > 40$ days
786 are highly underestimated. The model fits of the Ba isotopic composition of source and sink
787 (e, f) agree well with the experimental data in all three scenarios.
788
789 Fig. 5. Ba concentration data of the 1.0 M/10 °C diffusion experiment fitted with the
790 diffusive transport model with varying values for porosity (ϕ) and tortuosity (τ) of the silica
791 hydrogel, summarised as $u = \phi * \tau$. (a) Data fit of the source slightly improves with lower
792 values for u. At the same time, the effective diffusion coefficient has to increase. (b)
793 Evolution of the Ba concentration in the sink reservoir is independent of u, resulting in
794 identical concentration profiles.
795

Fig. 6. Effective diffusion coefficients extracted from the diffusive transport model with adsorption (white symbols) and without (grey/black symbols). The effective diffusivities correlate positively with temperature and $BaCl_2$ concentration. Reference salt diffusion coefficients of 0.1 M and 1.0 M $BaCl_2$ solutions at 25 °C were taken from Robinson and Stokes (2002). For other temperatures, diffusion coefficients were extrapolated (solid lines) using the Stokes-Einstein equation (Li and Gregory, 1974) with water viscosity data from Robinson and Stokes (2002).

Fig. 7. Ba isotopic composition of the sink reservoir of the 1.0 M/10 °C diffusion experiment fitted with different values for β. All data fall within a range of ±0.002 (grey area), which is taken as estimated uncertainty of β.

Fig. 8. Plot of β values of alkali and alkaline earth metals against diffusivity. β values were either experimentally derived (diamonds; Bourg et al., 2010; Richter et al., 2006) or calculated by MD simulations (circles; Bourg et al., 2010). Diffusion coefficients are for infinite dilution and 75 °C, calculated using the Stokes-Einstein equation with salt diffusion coefficients at 25°C and water viscosity data taken from Robinson and Stokes (2002).

Figure 1

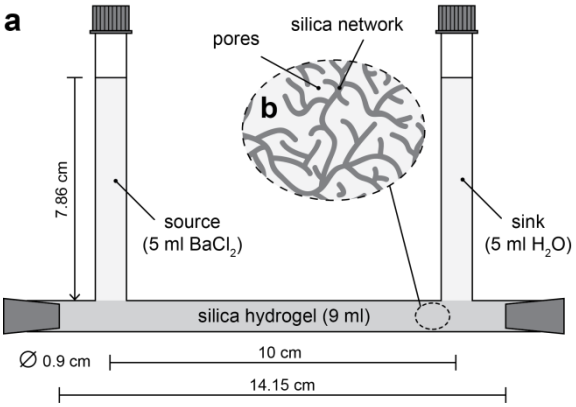
a
pores
silica network
b
7.86 cm
source
(5 ml BaCl2)
sink
(5 ml H2O)
silica hydrogel (9 ml)
∅ 0.9 cm
10 cm
14.15 cm

Figure 2

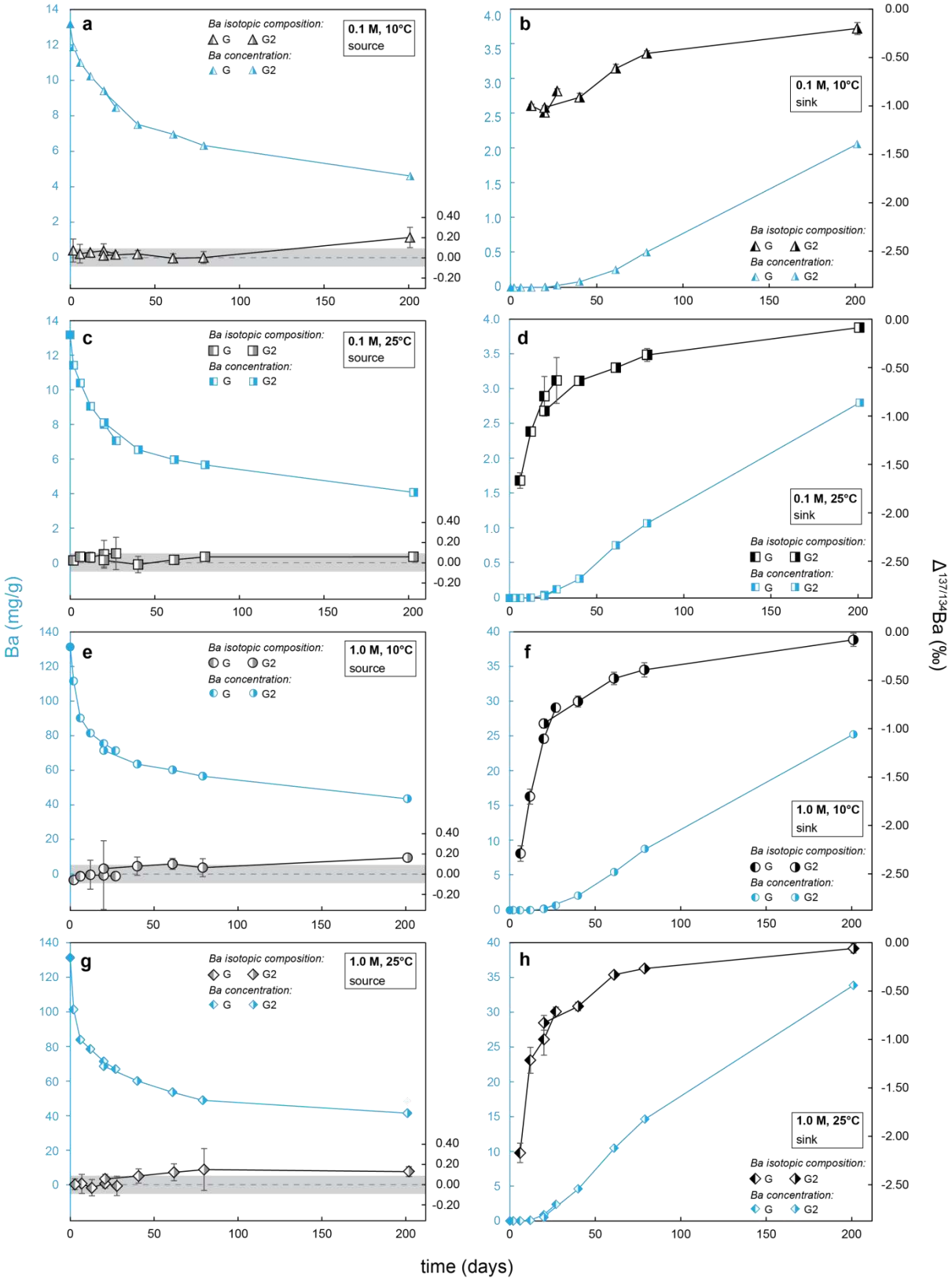
a
Ba isotopic composition:
G G2
Ba concentration:
G G2
0.1 M, 10°C
source
b
0.1 M, 10°C
sink
c
0.1 M, 25°C
source
d
0.1 M, 25°C
sink
e
1.0 M, 10°C
source
f
1.0 M, 10°C
sink
g
1.0 M, 25°C
source
h
1.0 M, 25°C
sink
Ba (mg/g)
Δ137/134Ba (‰)
time (days)

Figure 3

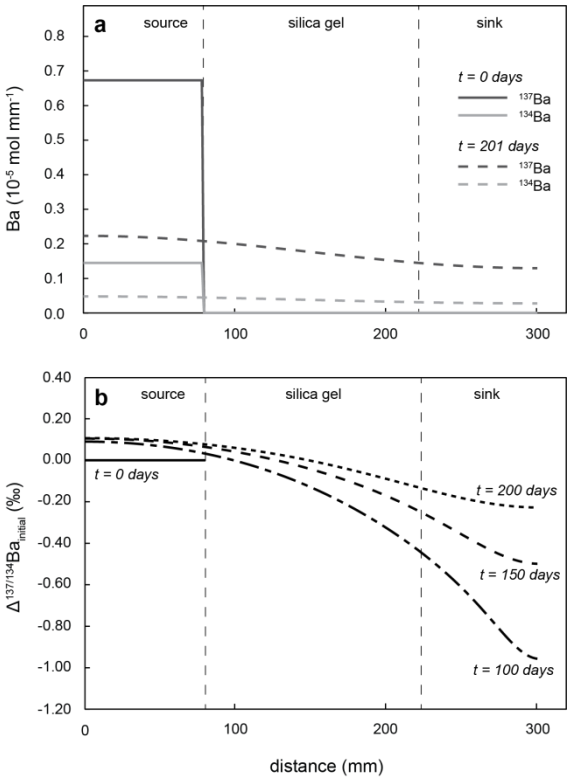
a
source
silica gel
sink
t = 0 days
137Ba
134Ba
t = 201 days
137Ba
134Ba
Ba (10-5 mol mm-1)
0.8
0.7
0.6
0.5
0.4
0.3
0.2
0.1
0.0
0
100
200
300
b
source
silica gel
sink
t = 0 days
t = 200 days
t = 150 days
t = 100 days
Δ137/134Bainitial (‰)
0.40
0.20
0.00
-0.20
-0.40
-0.60
-0.80
-1.00
-1.20
0
100
200
300
distance (mm)

Figure 4

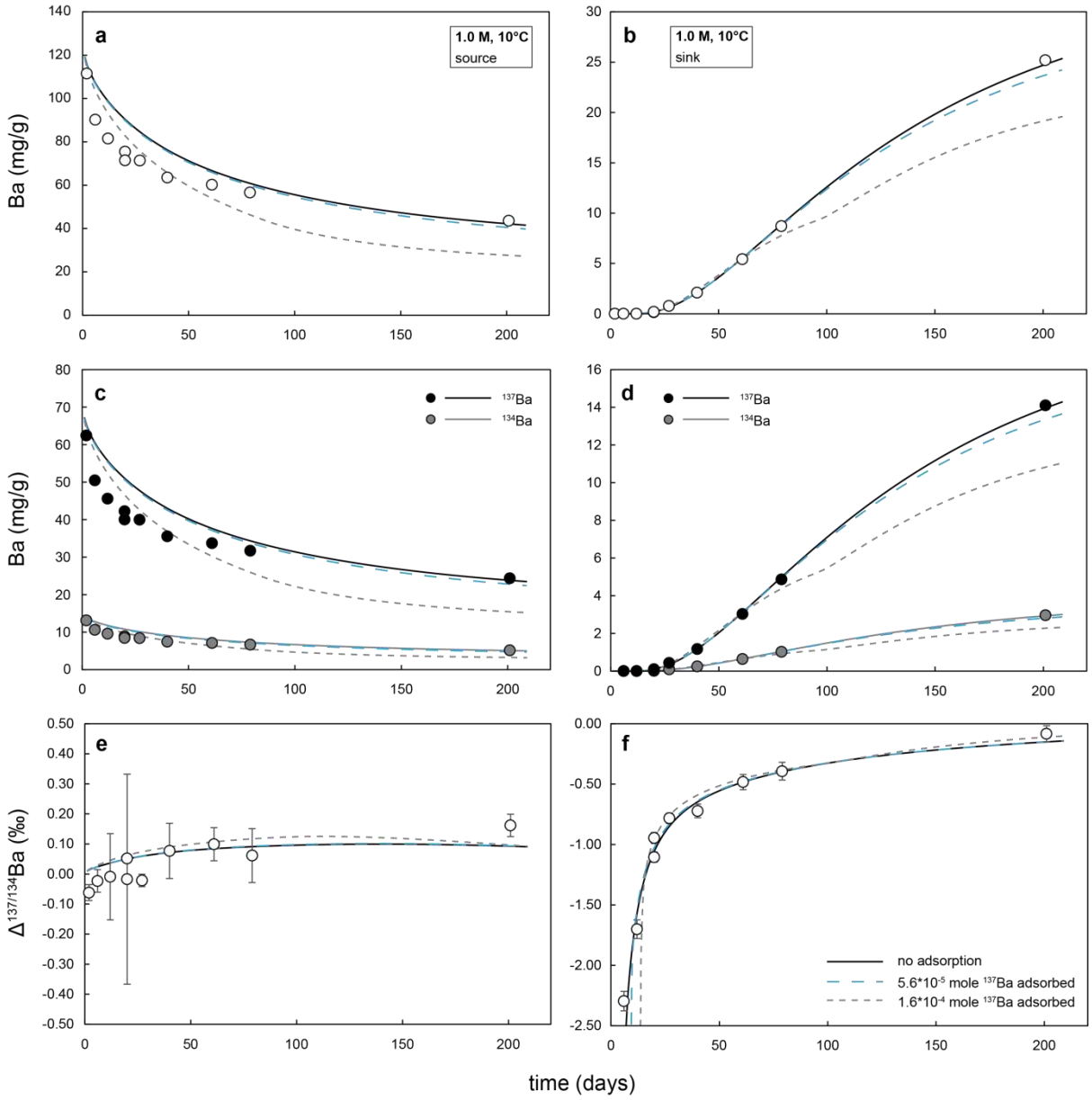
a
1.0 M, 10°C
source
b
1.0 M, 10°C
sink
c
d
^{137}Ba
^{134}Ba
e
f
Ba (mg/g)
$\Delta^{137/134}$Ba (‰)
time (days)
no adsorption
5.6*10^{-5} mole ^{137}Ba adsorbed
1.6*10^{-4} mole ^{137}Ba adsorbed

Figure 5

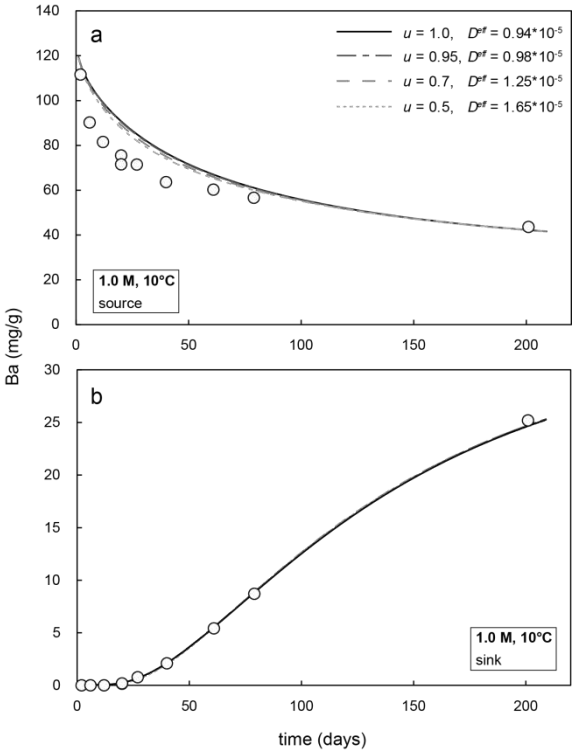

Figure 6

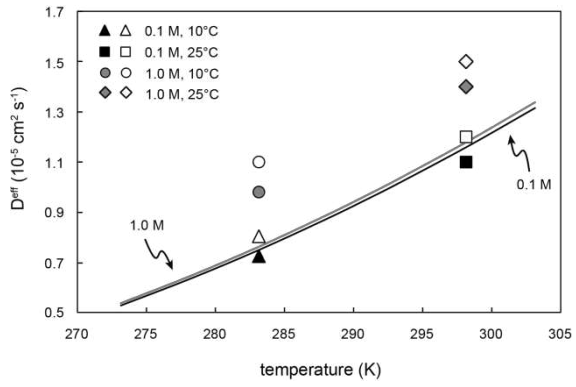

Figure 7

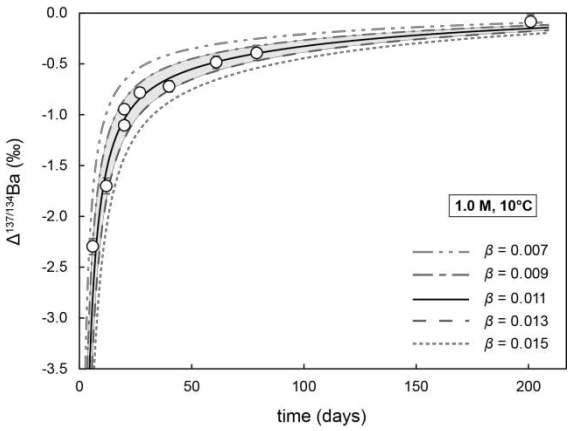

Figure 8

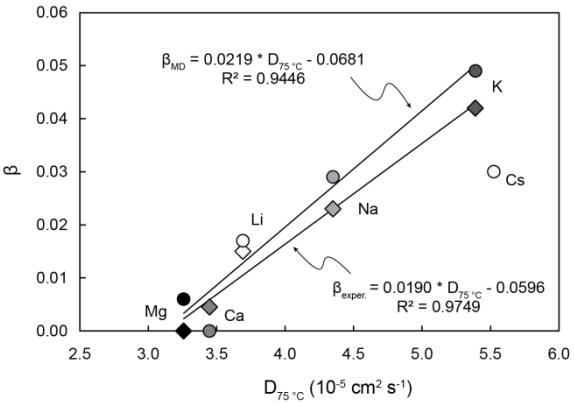

Supplementary information of:

Experimental determination of barium stable isotope fractionation during diffusion and adsorption at low temperatures

Kirsten van Zuilen [a,*], Thomas Mueller [b], Thomas F. Nägler [a], Martin Dietzel [c] and Tim Kuesters [b]

[a] Institute of Geological Sciences, University of Bern, Baltzerstrasse 1+3, 3012 Bern, Switzerland
[b] Institute of Geophysics and Tectonics, School of Earth and Environment, University of Leeds, Leeds, LS2 9JT, UK
[c] Institute of Applied Geosciences, Graz University of Technology, Rechbauerstraße 12, 8010 Graz, Austria

*Corresponding author: kirsten.vanzuilen@geo.unibe.ch
Present address: Institut de Physique du Globe de Paris, 1 rue Jussieu, 75238 Paris cedex 05

Diffusive transport model – data fit

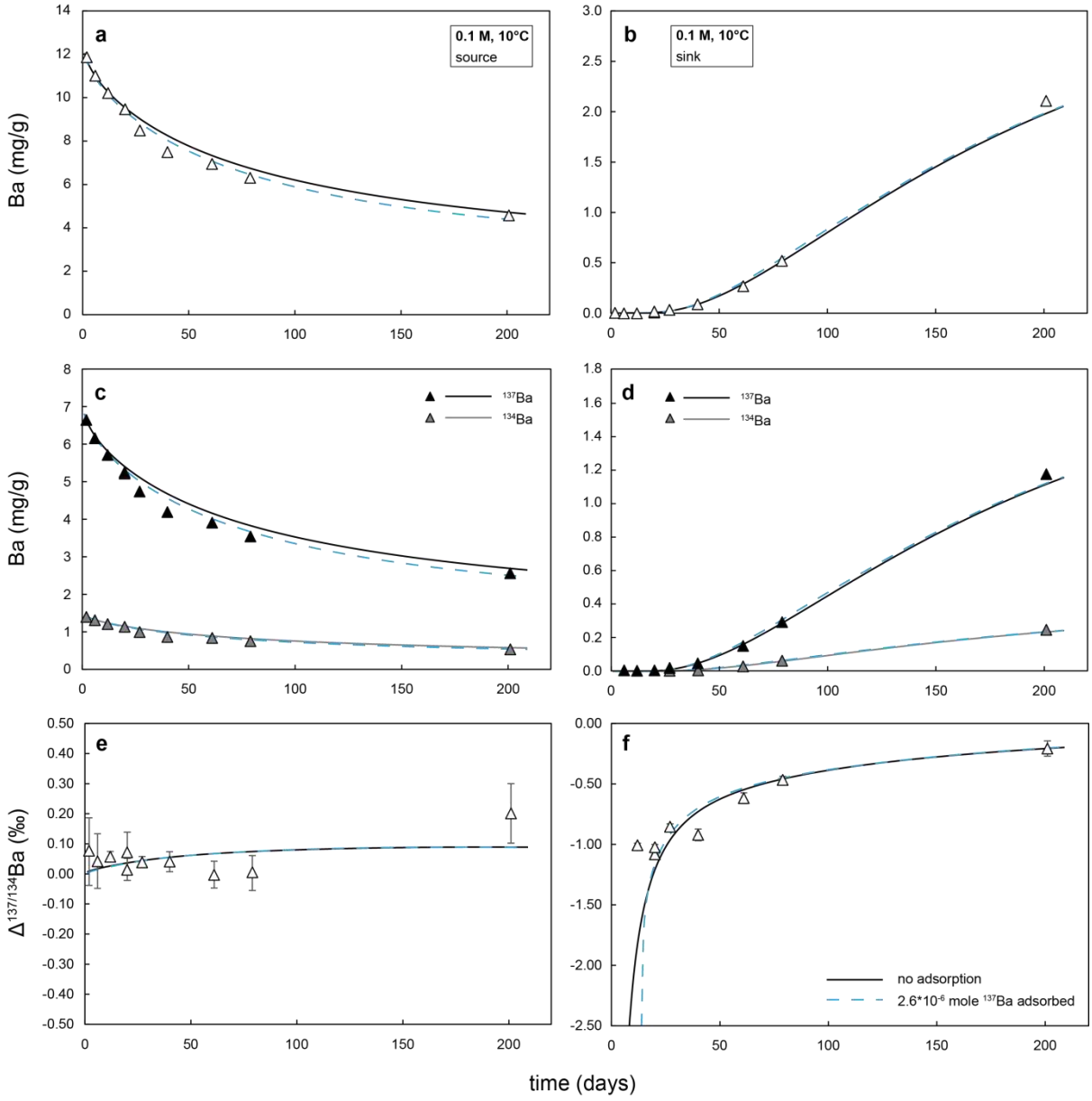

Fig. S1. Fit of experimental concentration and isotope data of the 0.1 M/10 °C diffusion experiment with the diffusive transport model with u = 0.95 with time. Measured and modelled data of the source reservoir are shown on the left hand side, data of the sink on the right hand side. 2 sd uncertainties of concentration data are smaller than symbol size. Shown are model runs without adsorption (solid lines) and with linear adsorption of maximum 2.6x10^{-6} moles ^{137}Ba and saturation of the gel surface after about 100 days (blue dashed lines).

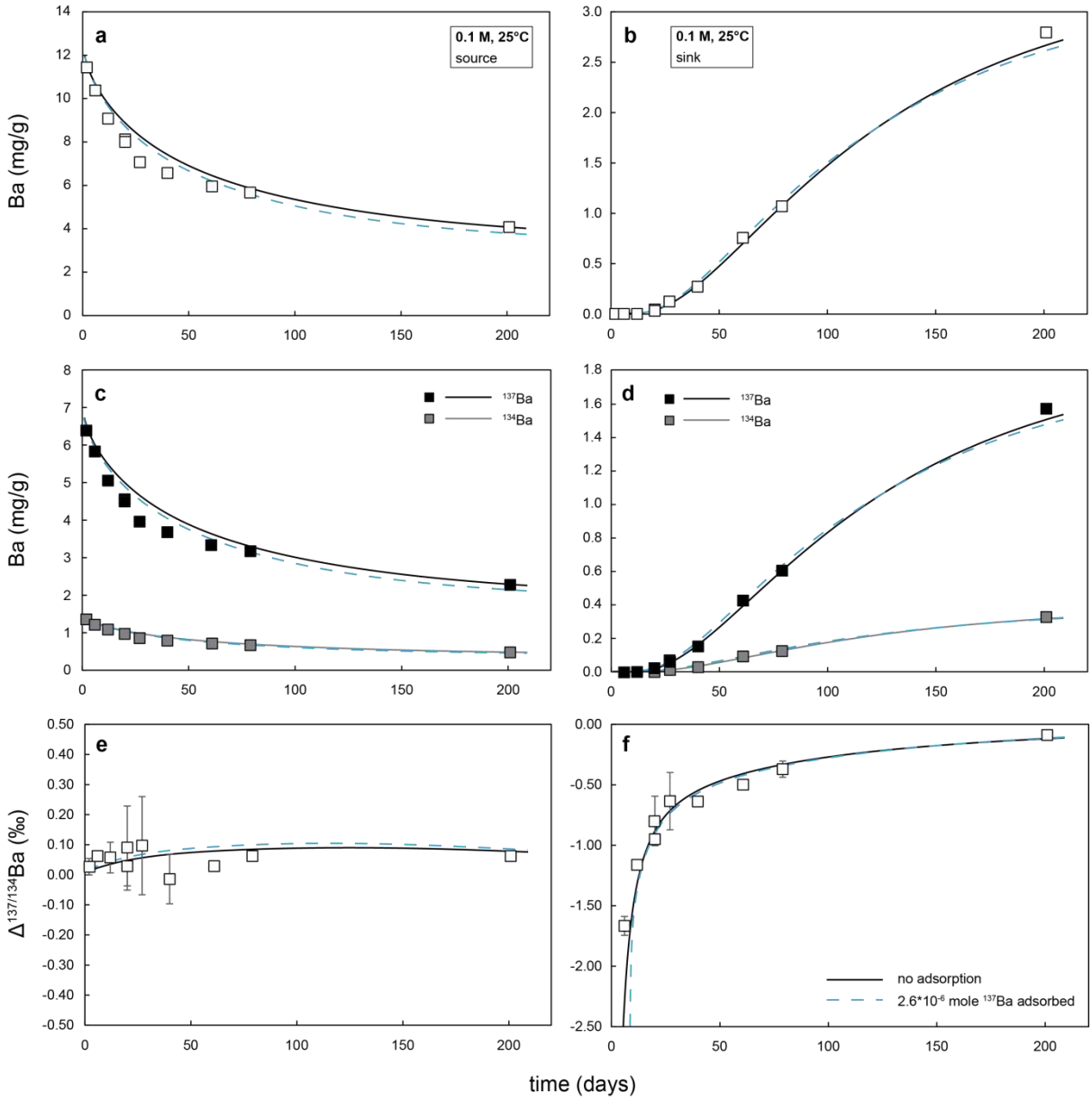

Fig S2. Same as Fig. S1 for the 0.1 M/25 °C diffusion experiment.

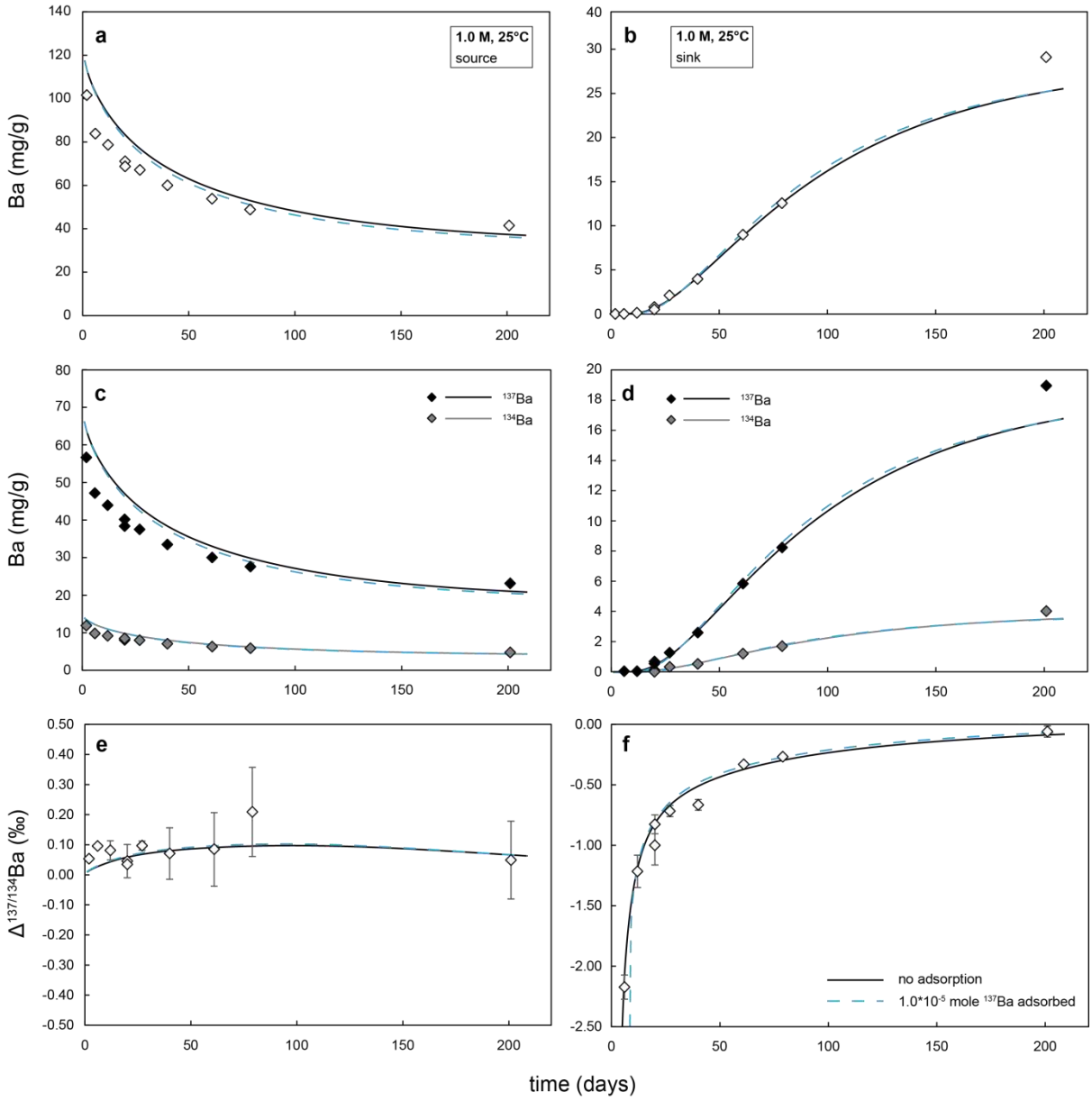

Fig S3. Same as Fig. S1 for the 1.0 M/25 °C diffusion experiment. Maximum of linear adsorption was 1.0×10^{-5} moles ^{137}Ba.

Multicomponent diffusion

The numerical model developed in this study calculates the mass-dependent diffusive transport and fractionation of two isotope species including additional isotope fractionation through adsorption onto the surface of the silica gel. It also accounts for spatial differences in the effective diffusivity arising from porosity and tortuosity affecting the reservoir filled with silica gel, but not the source and sink reservoirs. However, the effect of other components (e.g. Na or Cl) on the effective diffusion coefficient is not being considered in the present numerical solution. In other words, our model does not account for the effect of multicomponent diffusion.

Implementation of multicomponent diffusion in the numerical model is beyond the scope of this study. However, to test whether this may significantly bias our modelling results, we first developed a simplified multicomponent diffusion model using the publically available software package PHREEQC (Parkhurst and Appelo, 2013). The model uses the same geometry consisting of three reservoirs resembling source, silica gel and sink as well as their dimensions (Fig. 1, main text). Na^+ and Cl^- are released into the pore fluids of the silica hydrogel during gel formation. We thus consider Ba^{2+}, Na^+ and Cl^- as interacting diffusing species. The sink is set to be pure water, i.e., initially being free of any species considered here. The initial concentration profiles are based on estimated Na and Cl concentrations in the silica gel as well as on nominal Ba concentrations of 1.0 M and 0.1 M $BaCl_2$ in the source reservoir, respectively (Table S1). We emphasize that no porosity, tortuosity or adsorption is taken into account, making this a simple isothermal multicomponent aqueous diffusion model in one dimension. We are using the advective-dispersive-diffusive transport modelling routine implemented in PHREEQC, which solves the transport equation using an explicit finite difference scheme. In the present case, advective flow and dispersion are set to zero. Hence, molecular diffusion is the only operating transport mechanism, similar to our numerical code. The PHREEQC routine allows computing either the simple case of diffusive transport using one specific diffusion coefficients for all aqueous species involved or calculating the effective diffusion coefficient for each species based on their interaction using the multicomponent approach. According to multicomponent diffusion theory, the effective diffusion coefficient of a single species depends on its tracer diffusion coefficient and the electrical field resulting from differences in tracer diffusion coefficients between all involved species. In its simplest case, the effective flux J_i of species i can be described by an equation of the form (Boudreau et al., 2004):

$$J_i = -D_i \frac{\partial n_i}{\partial x} + z_i D_i E^* n_i \qquad \text{(S1)}$$

Here, the diffusive flux is being computed not only as function of tracer diffusion coefficient D_i and concentration gradient $\partial n_i/\partial x$ of a species, but also based on charge balance requirements represented by the second term, where z_i indicates the charge of the diffusing species and E^* the generated electrical field. Thermodynamic data for the PHREEQC model and tracer diffusion coefficients are taken from the 'phreeqc.dat' database (Table S1).

Table S1. Initial concentrations of source, sink and gel reservoir and tracer diffusion coefficient for the involved aqueous species at 25 ℃, originally published by Li and Gregory (1974)

species	concentration source (mol l^{-1})		concentration gel (mol l^{-1})		concentration sink (mol l^{-1})		D_i (10^{-5} cm^2 s^{-1})
	0.1 M $BaCl_2$	1.0 M $BaCl_2$	0.1 M $BaCl_2$	1.0 M $BaCl_2$	0.1 M $BaCl_2$	1.0 M $BaCl_2$	
Na^+	0.00	0.00	0.86	0.86	0.00	0.00	0.848
Cl^-	2.00	0.20	0.86	0.86	0.00	0.00	1.330
Ba^{2+}	1.00	0.10	0.86	0.86	0.00	0.00	2.030

The discrepancies between our numerical transport model and the measured Ba concentration data in the source are largest for the first 40 days of the diffusion experiments (Figs. 4, S1-S3). Thus, we limit the multicomponent diffusion model to the first 20 days and compare the resulting concentration profiles with predicted profiles resulting from independent Ba diffusion, as assumed in our numerical approach. The initial concentration profiles for Na, Cl and Ba exhibit different concentration gradients between the reservoirs for each element (Fig. S4). Consequently, different net diffusive fluxes in different directions will occur for the different species during homogenization. More specifically, Ba^{2+} will be diffusing in one direction from sink to source (Fig. S4c and f), while Na^+ is diffusing from the gel into both sink and source reservoirs (Fig. S4a and d). The partial counter flux of Na^+ with respect to Ba^{2+} then needs to be charge balanced by the diffusive flux of Cl^- in the medium. For Cl^-, resulting fluxes have to be considered separately for the two different starting source concentrations, i.e., 1.0 M and 0.1 M $BaCl_2$, respectively. In the case of high initial Cl concentration, a step-like initial profile is created and, consequently, Cl^- generally diffuses from the source and the gel reservoirs towards the sink (Fig. S4e). The model considering the 0.1 M $BaCl_2$ solution, in contrast, starts with an initial Cl distribution that has its maximum in the gel reservoir and an intermediate Cl concentration in the source (Fig. S4b). This results in a net flux of Cl^- into both sink and source reservoirs.

As a consequence, Na concentration profiles after 20 days are asymmetric, showing slightly faster net diffusive fluxes into the sink reservoir. This is in agreement with the predicted flux directions, as Na^+ and Cl^- are diffusing simultaneously into the sink reservoir which is filled with pure water. At the other end, dependent on the initial $BaCl_2$ concentration in the source, either

Ba^{2+} (0.1 M experiments) or Ba^{2+} and Cl^- (1.0 M experiments) diffuse from the source into the gel reservoir with a counter flux of Na^+ into the source. Charge balance requirements link the effective fluxes of the cations to the evolving concentration profiles of Cl^-, resulting in a slightly lower net diffusive flux of Na^+ into the source reservoir for the 1.0 M $BaCl_2$ run. Anion and cation fluxes in the 0.1 M $BaCl_2$ run are similarly linked. Due to the lower $BaCl_2$ concentration, however, all multicomponent effects are weaker or even reversed in regions with different flux directions, i.e., from gel reservoir into the source or vice versa. The concentration dependence of the multicomponent effect is predicted by Eq. S1, as the charge compensation term is directly proportional to the concentration of the species. Modelled profiles for Ba are exclusively affected by the coupling process between the source and the gel reservoir. For high initial Ba concentrations, a slightly faster effective diffusive flux of Ba^{2+} out of the source (Fig. S4f) is driven by the migration of Cl^- into the gel. On the other hand, effects of multicomponent diffusion on the Ba profile in the 0.1 M Ba run are virtually not visible (Fig. S4c).

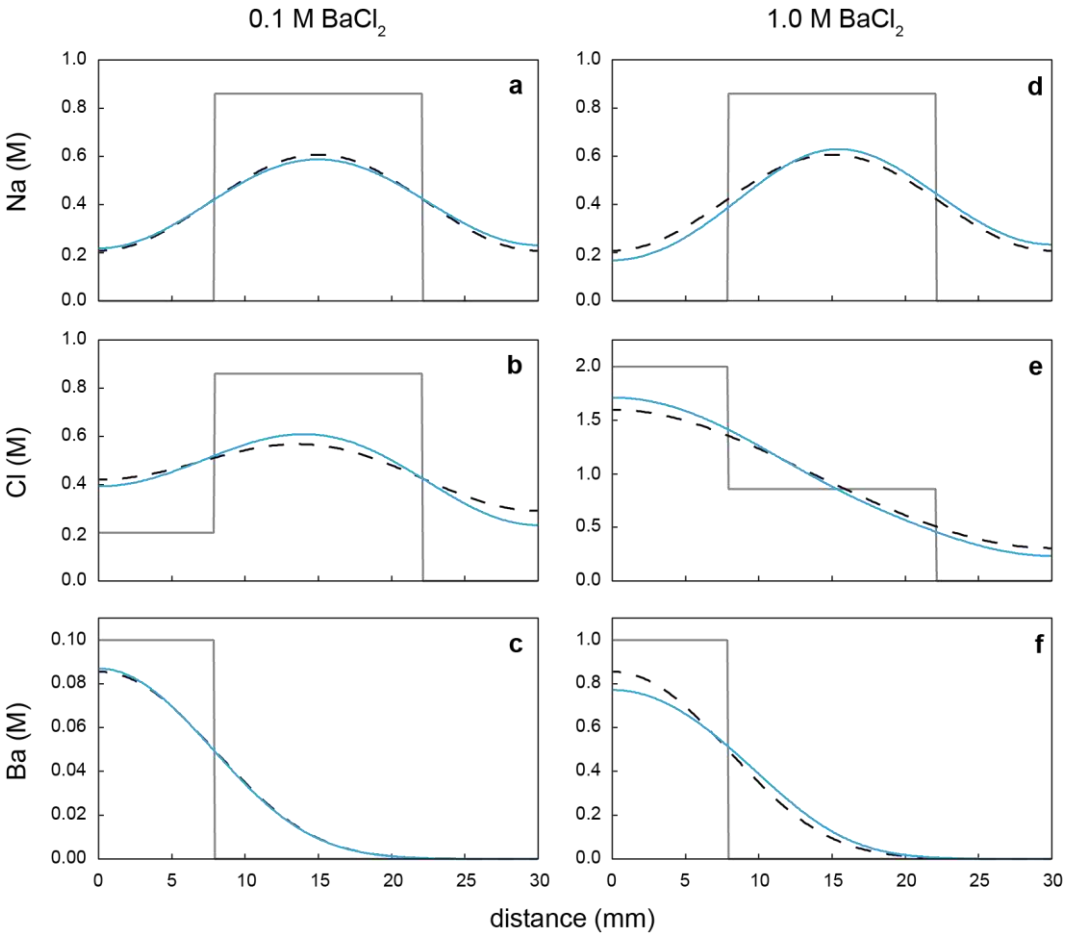

Fig. S4. Multicomponent diffusion. Grey solid lines: initial concentration profiles for Na, Cl and Ba; blue solid line: concentration profiles for multicomponent diffusion after 20 days; black dashed lines: concentration profiles for one-component diffusion after 20 days.

References in Supplement

Boudreau, B. P., Meysman, F. J. R., Middelburg, J. J. (2004) Multicomponent ionic diffusion in porewaters: Coulombic effects revisited. Earth and Planet. Sc. Lett. **222**, 653-666.

Li, Y.-H., Gregory, S. (1974) Diffusion of ions in sea water and in deep-sea sediments. Geochim. Cosmochim. Acta **88**, 708-714.

Parkhurst, D. L. and Appelo, C. A. J. (2013) Description of input and examples for PHREEQC version 3: a computer program for speciation, batch- reaction, one-dimensional transport, and inverse geochemical calculations. In Modeling Techniques. U.S. Geological Survey, Reston, 6-A43.